5-2015

Stratigraphy and Depositional Environment of the Mesaverde Group in the Northern Bighorn Basin of Wyoming

Gordon Adams
University of Nebraska-Lincoln, gordon.adams@huskers.unl.edu

STRATIGRAPHY AND DEPOSITIONAL ENVIRONMENT OF THE MESAVERDE GROUP IN THE NORTHERN BIGHORN BASIN OF WYOMING

by

Gordon Adams

A THESIS

Presented to the Faculty of

The Graduate College at the University of Nebraska

In Partial Fulfillment of Requirements

For the Degree of Master of Science

Major: Earth and Atmospheric Sciences

Under the Supervision of Professor Christopher R. Fielding

Lincoln, Nebraska

May, 2015

STRATIGRAPHY AND DEPOSITIONAL ENVIRONMENT OF THE MESAVERDE GROUP IN THE NORTHERN BIGHORN BASIN OF WYOMING

Gordon Adams, M.S.

University of Nebraska, 2015

Advisor: Christopher R. Fielding

A sedimentological, stratigraphical and palynological study was conducted on the upper Cretaceous (Campanian) Mesaverde Group over 27.5 km of a north-south-orientated outcrop belt in the northern Bighorn Basin, Wyoming. During the Campanian, the study area lay in the western part of the Cretaceous Western Interior Seaway. The study aims to provide a stratigraphic and paleoenvironmental analysis of the Mesaverde Group and to integrate findings with data from outcrop belts to the south (southern Bighorn Basin), north (Montana) and east (Powder River Basin).

The Mesaverde Group (371 - 515 m thick) comprises a succession of mainly coarsening-upward stratal cycles, with some anomalous, sharply-based sandstone bodies that are out of context with respect to underlying facies. The trace fossil assemblage is typically of low diversity with only a few ichnotaxa recurring throughout the succession. The palynofacies analysis shows predominantly low abundance of palynomorphs and dinoflagellates indicating a high energy environment. There is, however, a wide range in types and abundance of phytoclasts present. Paleocurrent data indicate a dominantly southeastward direction of sediment dispersal with bi-modal sediment dispersal patterns within individual facies.

This study indicates a similar lithological assemblage to previous studies of the Mesaverde Group; however the interpretation of depositional environment from this study points towards a dominantly deltaic depositional environment, something that only a subset of previous studies has done. The depositional environment changes vertically throughout the section from distal to proximal, with facies associations ranging from basinal to coastal plain. The palynofacies analysis performed in this study is consistent with the lithofacies analysis but also reveals some flooding events that are not revealed by the lithology. Finally, four sequence stratigraphic cycles are interpreted throughout the Mesaverde Group identified by incised lithosome bases and major dislocation of facies. Overall this study provides a basis for future study on the Mesaverde Group and allows for a more detailed paleoenvironmental evaluation of the unit.

Acknowledgements

This thesis would not have been possible without the help of many people to whom I am forever grateful and indebted. First and foremost I want to thank Dr. Christopher Fielding who has been a source of invaluable assistance, information and advice since this project began. Without his patience, knowledge and mentorship I would not have gotten this far. I'd also like to thank my wife Kristen who has helped me with all the images in this document, and who worked tirelessly to assist me in the field. To my parents, family, and my closest friends in both Scotland and Nebraska for their guidance and support throughout this study, with a special thanks to Sebastian Blanchard for helping Dr. Fielding gather palynological samples for me. I'd also like to thank my colleague Andrew Hutsky for his advice and friendship. I want to thank Mr. and Mrs. Casey for allowing me access to their land and arranging access to their neighbors' land which is part of the study area. I also thank Dr. Oboh-Ikuenobe and Mr. Robert Haselwander, at the University of Missouri, Rolla, without whom the palynological aspect of this study would not have been possible. To Dr. Tracy Frank and Dr. David Watkins for agreeing to be my committee members and for providing me with abundant help over the course of this project. Finally, I'd like to acknowledge the Department of Earth and Atmospheric Sciences at the University of Nebraska Lincoln for the opportunity to carry out graduate research and for the funding it provided me through a TA position and a fellowship to allow me to follow my dream.

Table of Contents

Introduction

The Mesaverde Group has been studied in detail throughout the western United States and Canada but has not been documented in detail in the northern Bighorn Basin of Wyoming; this study will investigate these poorly studied outcrops. The purpose of this study is threefold. First, a stratigraphical and lithological analysis of the poorly studied Mesaverde Group of the northern Bighorn Basin in Wyoming will be conducted in order to produce both a paleoenvironmental and stratigraphical analysis of the Mesaverde that can be compared against previous studies. Second, a palynofacies analysis of the group will be integrated into the paleo-environmental analysis to achieve a higher resolution evaluation of depositional environments. Finally, the results will be compared to previous studies on contemporary formations in Wyoming's southern Bighorn Basin and the Powder River Basin in eastern Wyoming for a more comprehensive overview of the Mesaverde Group. This study will facilitate a fuller understanding of Mesaverde Group stratigraphy to inform future studies.

The Mesaverde Group in the Western Cordilleran Foreland Basin of North America is an important stratigraphic unit because of its resource potential. Component formations are known to host not only coal deposits, which have been extensively mined, but also large quantities of shallow biogenic gas which has become of interest in hydrocarbon exploration in recent years (Condon 2000). The Mesaverde Group has been studied in detail in many regions of the United States, but the unit in the northern Bighorn Basin of north central Wyoming has not been studied in the modern era. There have been a few localized studies of the formation (e.g., Johnson et al. 1998); however no study has considered the outcrop belt as a whole. There have been a number of stratigraphic studies

in adjacent areas. In Montana, studies by Condon (2000), Rice (1980), and Roehler (1990) have been published. Studies in the southern Bighorn Basin include Severn (1961) and Fitzsimmons & Johnson (2000) and to the east in the Powder River Basin, Purcell (1960), Rich (1958) and Crews et al. (1976).

The most commonly accepted stratigraphic division is into four members, from base to top: the Eagle Formation, the Claggett Shale Member, the Judith River Formation and the Teapot Sandstone Member. The Mesaverde Group is underlain by the Cody Shale and overlain by the Meeteetse Formation (Fig.1). The range of depositional environments represented within the Mesaverde Group has been discussed in previous studies; interpretations range from offshore marine, through deltaic, to multistory coastal platform fluvial/tidal channels (Fitzsimmons & Johnson 2000), and also include barrier islands and protected lagoons (Kieft et al. 2011).

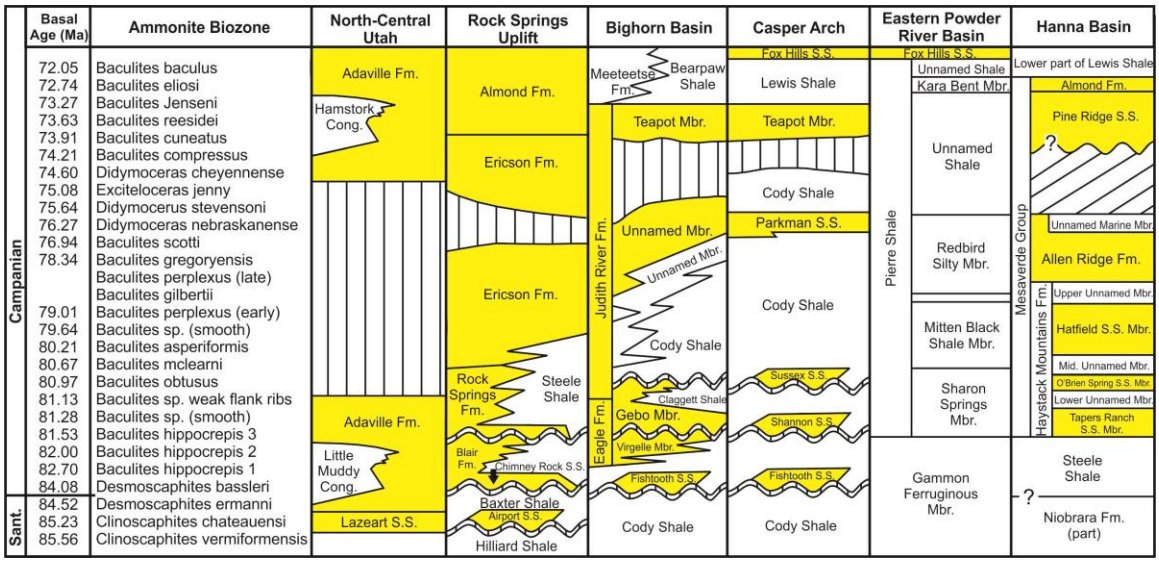

Figure 1: Regional stratigraphic frame work of the Campanian strata of Wyoming. Fm stands for formation, SS for sandstone, and Mbr for member. Sandstones are shaded in yellow. Modified from Swift et al. (2008) & Martinsen et al. (1995).

Geologic Setting

The Mesaverde Group accumulated within the Cretaceous Western Interior Seaway during the late Cretaceous (Campanian to Maastrichtian), approximately 83 -76 Ma (Gill & Cobban 1966). The timing of Mesaverde Group accumulation is constrained by the presence of temporally significant ammonite marker species. The base of the Mesaverde Group fall within a biozone defined by *Scaphites hippocrepis* (82.7 Ma) and the top by *Baculites cuneatus* (73.91 Ma) (Gill & Cobban 1973) (Fig.1). The Mesaverde Group is composed of two main sandstone wedges encased in marine mudrocks, formed within a retroarc foreland basin. The sands were derived from the erosion of the Sevier Orogenic Belt to the west of the basin (Jacka 1965). These two wedges are believed to record eastward progradation of deltaic/shallow marine systems into a shallow marine basin (Severn 1961; Condon 2000; Fitzsimmons & Johnson 2000). There are also a number of thin sandstone bodies within the group.

The Bighorn Basin is a Laramide (Cenozoic) syncline surrounded by basement-cored mountain ranges (Fig. 2). It preserves a thick Cretaceous succession; however, it formed in the Western Cordilleran Foreland Basin during the earlier Sevier Orogeny. The exposure of the Mesaverde within the Bighorn Basin is facilitated by the presence of numerous valleys and shallow dipping strata that allow for excellent exposure of the differing lithologies of the Mesaverde Group (Fitzsimmons & Johnson 2000).

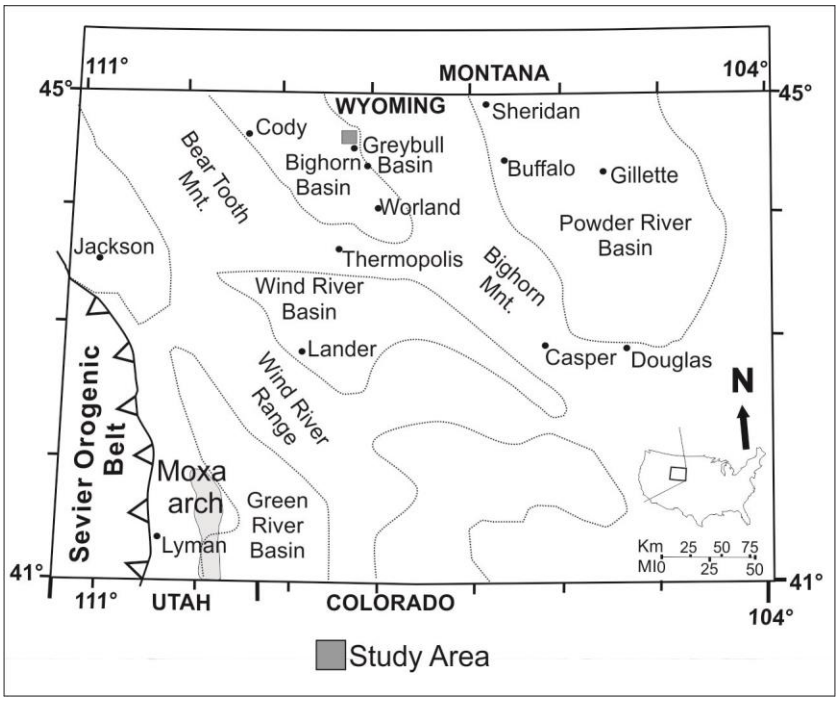

Figure 2: Map of Bighorn Basin in Wyoming, showing study area. Modified after Clark (2010).

Previous Research

The thickness of the Mesaverde Group in previous studies ranges from 300 - 800 m thick. The nomenclature of the Mesaverde Group varies from region to region, although internally the stratigraphy is laterally persistent between regions. As summarized above, the Mesaverde Group is divided into four component units (Fig. 1). The Mesaverde Group is underlain by the Cody Shale and overlain by the Meeteetse Formation.

The underlying Cody Shale comprises dark fissile shale locally interbedded with fine-grained sandstone. The percentage of sandstone in the Cody Shale increases upward through the succession. Bentonite beds are common near the top of the Cody Shale. The contact between the Cody Shale and the Eagle Formation is identified as gradational in some locations (Severn 1961; Condon 2000), but sharp based in others (Keefer et al. 1998).

The stratigraphic nomenclature in used in Wyoming derives from studies in the adjacent state of Montana. The lowermost formation of the Mesaverde Group is the Eagle Formation (Fig. 1) which has been defined as a fine to very fine grained sandstone interbedded with muddy sandstone (Severn 1961; Condon 2000). The upper part of the unit, referred to as the Gebo Member, also contains interbedded carbonaceous shales, claystones, and thin lenticular sandstone beds. The thickest body of sandstone present is referred to as the Virgelle Member. In Montana, the Eagle Formation overlies the Telegraph Creek Formation, which is not formally recognized in Wyoming (Fig. 3). The Telegraph Creek Formation is the lower mudrock member and the Eagle Sandstone is the upper, more sand rich unit (Fig. 3). Previous studies such as Condon (2000) and Roehler (1990) have reported the thickness of the Eagle Formation as 61 - 152 m. The upper contact with the Claggett Shale Member is abrupt and believed to be unconformable with shale of marine origin directly overlying deposits of continental origin (Severn 1961; Condon 2000).

The second member in vertical succession of the Mesaverde Group is the Claggett Shale (Claggett Shale Formation in Wyoming) (Figs. 1 & 3). The Claggett Shale Member has a thickness range of 61 - 152 m. Its composition near the base is shale with interbedded siltstone and sandstone. The member coarsens upwards with sandstone becoming the dominant lithology towards the top. This sandstone has locally been named the Claggett Sandstone (Swift et al. 2008) or the Parkman Sandstone in southern Wyoming (McGookey et al. 1972) (Fig. 1). The contact between the Claggett Member and the overlying Judith River Formation is both gradational and conformable.

The Judith River Formation (Fig. 1) is composed of sandstones, siltstones, coals and shales. Sandstone beds are as much as 20 m thick in some areas. The sandstones range from fine- to coarse-grained (Severn 1961; Condon 2000). The thickness of the Judith River Formation ranges from 30 – 182 m. The contact with the overlying formations varies from east to west. In the east, the Judith River Formation is conformably overlain by the Bearpaw Formation and in the western outcrops is unconformably overlain by the Meeteetse Formation (Fig. 1).

The uppermost defined unit of the Mesaverde Group in the study area, the Teapot Member, of the Judith River Formation, is impersistent (Fig. 1). Where present, it is represented by thick, amalgamated sandstone. It has been described as a grey sandstone with some interbedded grey mudstone (Keefer et al. 1998). The thickness ranges from 30 – 60 m (Fig. 1). The contact with overlying formations is conformable with the previously described contact between the Judith River Formation and the overlying formations (Rich 1958; Purcell 1960; Crews et al. 1976; Martinsen et al. 1995).While the stratigraphic nomenclature of these units is largely consistent from region to region, interpretation of the depositional setting has varied. The Eagle Formation was identified by Condon (2000) in central and eastern Montana as non-marine to marine shelf sandstone; Fitzsimmons and Johnson (2000) have identified it as a deltaic deposit in the western Bighorn Basin. The Claggett Shale unit has been identified in studies as an offshore marine shale; this interpretation has not varied significantly throughout any of the previous studies. The depositional environment of the Judith River Formation and equivalent formations has been identified as both a non-marine to marginal marine transition (Condon 2000) in central and eastern Montana and a deltaic deposit in both the

Western Bighorn Basin (Fitzsimmons & Johnson, 2000) and South Central Wyoming (Martinsen et al. 1995). Finally, the Teapot Member and equivalent units where it has been recognized in studies by Fitzsimmons and Johnson (2000) and Martinsen et al. (1995), has been identified as estuarine (Fitzsimmons & Johnson 2000) in the Western Bighorn Basin and tidally influenced fluvial deposits in south central Montana (Martinsen et al. 1995). Overall, all interpretations have indicated depositional environments becoming more proximal upward through the succession. The biggest inconsistency in the interpretations is the influence of deltaic processes on the depositional environment of the Mesaverde Group.

Generalized Outcrop Stratigraphic Column for Central Montana

Era	System	Series	Formation		Thickness	Column	Lithology
Mesozoic	Creataceous	Upper	Montana Group	Bearpaw Fm.	800' - 1350'		Dark grey marine shale with numerous, fossiliferous, calcareous concretions. Bedding not prominent. Forms barren rounded slopes. Thickens eastwards into the Pierre Shale and thins westwards and becomes sandy into the continental Livingston Formation.
				Judith River Fm.	250' -500'		Inter-bedded light colored sandy shales, sandstones, and darker shales. Fresh water deposits often occur especially towards the top. Commonly has a hogback forming sandstone at the top and the base. Thins eastward and thickens westward.
				Claggett Fm.	200' - 300'		Primarily dark grey shales that weather reddish brown and contain relatively barren clacareous concretions, usually capped by a persistent shaley sandstone, referred to as the Parkman sandstone to the south. Thickens eastward and thins westward into the Livingston Formation.
				Eagle / Virgelle	200' - 525'		Thin bedded sandstones with interbedded shales and coals in the upper portion with massive white to buff sandstones at the base. Thins rapidly eastward and localy missing as a sandstone on the northeast flank of Cat Creek near Mosby and on the west flank of Porcupine Dome. Upper portion grades into the Livingston Formation to the west.
				Telegraph Creek Fm.	Variable		A transitional unit over much of the area becomes increasingly sandy upward.
			Colorado Group	Niobrara - Carlile			Homogeneous dark grey marine shale with calcareous concretions and a few bentonitic beds.

Figure 3: General stratigraphic column of the Campanian of Montana. Modified from Lawlor (1956).

Methods

A detailed sedimentological and ichnological analysis was performed along a 27.5 km northwest-southeast trending outcrop belt within the northern Bighorn Basin in Wyoming. Five outcrop sections were measured (Fig. 4); four during this study and one revisited from an earlier study by Fielding and Reiss in 2013. Due to the discontinuous nature of exposure and its condition, the spacing between the localities was variable. Outcrop sections were measured using a Jacob's staff, a compass/clinometer, a measuring tape and a digital range finder. A northwest-southeast cross section was constructed from the measured sections including those of Reiss (unpublished). Sedimentological and ichnological data and fossil samples were collected. Sedimentary structures, grain size trends, bed contacts, unit thickness, paleocurrent data and lateral and vertical trends in these properties were recorded for further analysis. A bioturbation index was used in which each rock is ascribed a value based on the degree of observed sediment destratification (Bann et al. 2008) (Fig. 5). Bioturbation values range from zero, complete absence of bioturbation, to six which indicates complete reworking of the sediment by biogenic processes (Bann et al. 2008). The thickness, lithologies and stacking patterns present were then compared to previous studies by Rich (1958), Purcell (1960), Severn (1961), Crews et al. (1976), Rice (1980), Roehler (1990),Condon (2000), and Fitzsimmons & Johnson (2000).

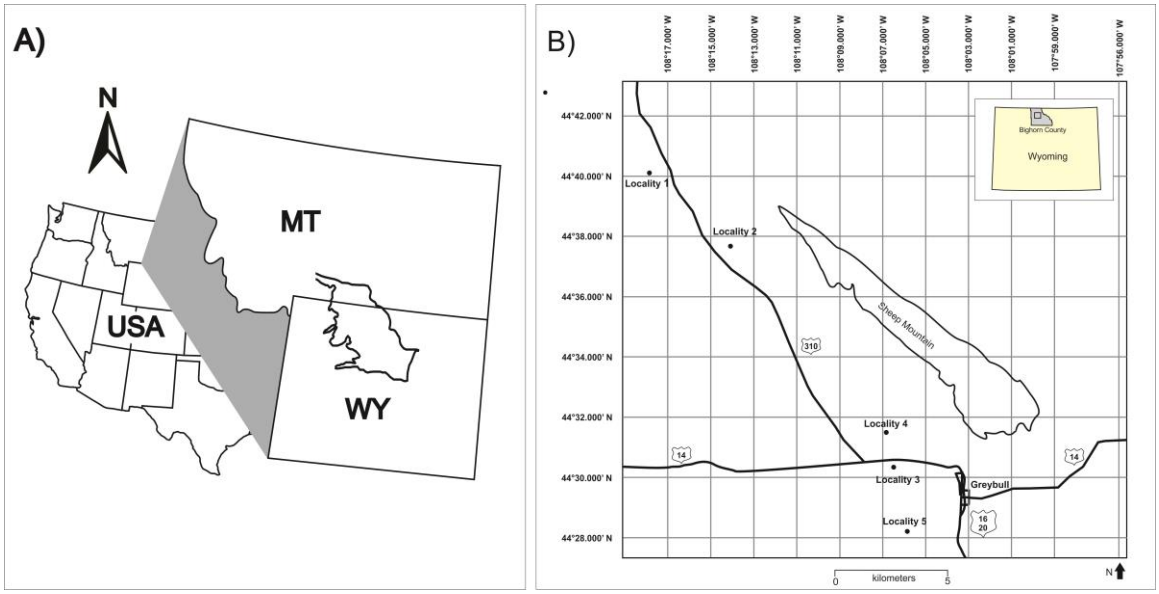

Locality	Base of Section	Top of Section
Locality 1	N 44° 40.147' W 108° 17.430'	N 44° 39.953' W 108° 17.777'
Locality 2	N 44° 37.573' W 108° 14.225'	N 44° 37.180' W 108° 14.402'
Locality 3	N 44° 30.096' W 108° 05.635'	N 44° 30.008' W 108° 06.233'
Locality 4	N 44° 27.997' W 108° 08.198'	N 44° 27.810' W 108° 05.711'
Locality 5	N 44° 31.235' W 108° 06.427'	N 44° 31.281' W 108° 06.623'

Figure 4: A: Regional map showing location of the Bighorn Basin. B: Local map of the study area within the Bighorn Basin showing location of the five measured sections along a 27.5 km northwest southeast transect. Palynological samples were taken from locality one.

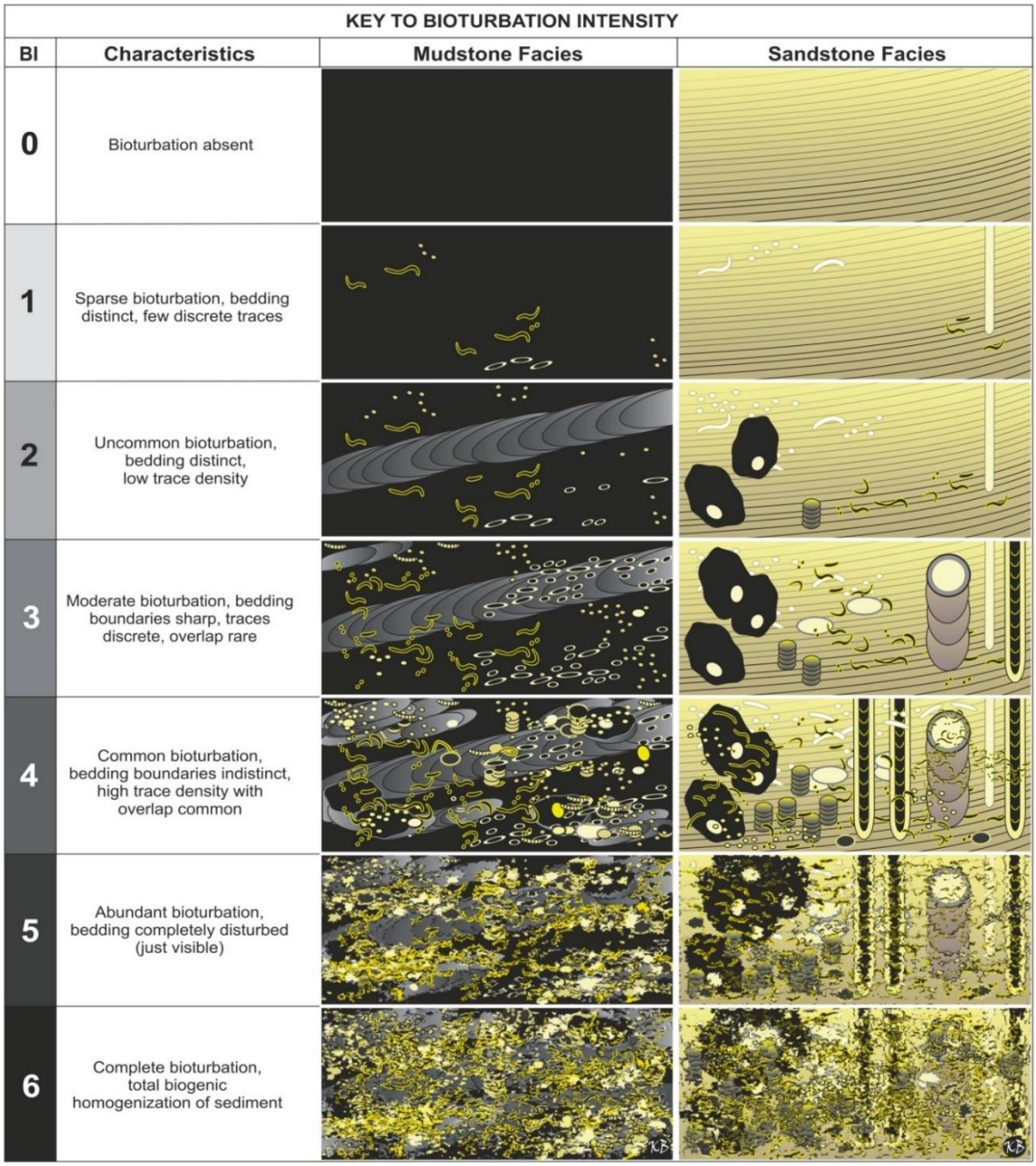

Figure 5: Bioturbation intensity key (Bann et al. 2008).

Twelve samples of fresh mudrock or carbonaceous mudrock were taken from surface exposures at locality one for palynological analysis. These were prepared using standard palynological slide preparation techniques. A palynofacies analysis based on a 300 point count was carried out on the produced kerogen slides. A 300 count was chosen due to the fact that it has a high statistical probability of identifying the complete variance of the assemblage (Dennison and Hay 1967) and it allows for the fact that some slides preserve only sparse assemblages. Palynomorphs and dispersed debris were counted using the classification scheme of Oboh-Ikuenobe (2005) (Table 2). The data produced from these counts were quantitatively analyzed using multiple methods including a principal components analysis (Hammer and Harper 2006), cluster analysis (Hammer and Harper 2006), Tyson Ternary Analysis (Tyson 1993) and factor analysis (Hammer and Harper 2006). Palynomorphs were identified using the work of Tschudy (1973).

Facies Associations

Facies seen within this study were identified based on several criteria: lithology, sedimentary structures, both the intensity and composition of the bioturbation and finally the facies position in relation to other facies. Using this information, interpretation of water depth, flow velocity and depositional regime could be ascertained. Facies seen throughout the study are described below; for bed thickness and detailed description of the facies refer to appendixes 1, 2, 3 and 4.

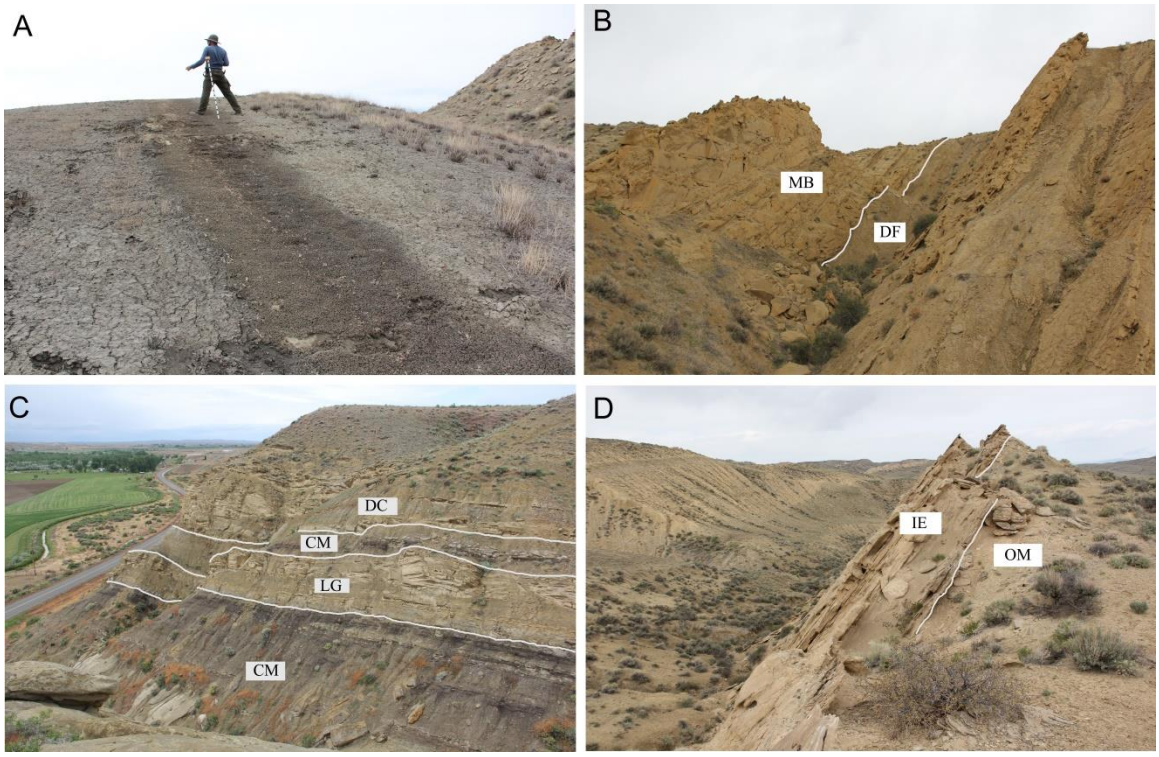

Figure 6: A: Basinal facies association showing offshore marine shales with interbedded bentonites. **B:** Delta front facies association represented by mouth bar deposits (MB) cutting down into finer-grained delta front deposits (DF). **C:** Coastal platform facies association with cyclical deposits of coastal mire deposits (CM) containing lagoonal deposits (LG) and finally erosionally based distributary channel deposits (DC). **D:** Incised estuary facies association shown with sharply-based incised estuary deposits (IE) directly overlying offshore marine deposits (OM).

Basinal Facies Association

Facies B1

Description

Facies B1 is dark grey to black, highly fissile shale containing minor, thin, discontinuous laminae of siltstone and sandstone (Fig. 6 A). Thin bentonite beds are present within this facies. This facies is present in the Cody Shale and the Claggett Shale across the entire study area (Appendix 1).

Interpretation

Facies B1 is interpreted as the deposits of a distal offshore marine environment. This is due to the abundance of fine-grained material likely deposited out of suspension from buoyant hypopycnal plumes. The sandstones

present are interpreted to be the product of high energy storm events. The lack of bioturbation within the facies indicates an anoxic environment hindering the development of a sustained invertebrate population. While fine grained lithologies deposited through suspension can be formed in both marine and lacustrine environments, the presence of marine fossils indicates offshore marine setting.

Facies B2

Description

Facies B2 is composed of shales with siltstone interbeds and laterally discontinuous sandstone lenses. Siltstone becomes more common upwards within intervals concomitant with coarsening and thickening upward trends. No physical structures are preserved in this facies, but carbonate concretions are present throughout and contain macerated ammonite fragments. Ammonite fragments are also preserved outside of the carbonate nodules. The bioturbation in this facies is restricted in diversity and abundance (Appendix 1).

Interpretation

Facies B2 is interpreted as proximal offshore marine deposits. Sediment was likely deposited from suspension out of hypopycnal plumes and from gentle bottom currents. There is evidence for some terrestrial influence into this facies with the presence of comminuted plant debris (Fig. 11 E) in some of the siltstone beds. The interpretation of a proximal offshore marine environment was based on numerous factors, notably the presence of ammonites which are exclusively marine fauna. The more proximal interpretation was reached due to an increase in terrestrial components such as sand and plant fragments that would have been

introduced to the system in storm events. This increase from the previous facies B1 indicates that it is more proximal.

Facies B3

Description

Facies B3 is composed of siltstone with thinly interlaminated and interbedded sandstone. Locally, thin discontinuous black fissile shale beds are present, as are carbonate concretions. The sandstones are sporadically bioturbated.

Interpretation

Facies B3 is interpreted as the product of a prodelta environment, which only the most energetic bottom currents could reach. The sandstone bodies were formed in such events. The finer-grained material was formed via suspension fallout from hypopycnal plumes, or from mud-bearing bottom currents (Appendix 1). The relationship of this fine grained facies to the overlying facies, both deltaic facies D1 and D2, indicates a prodelta facies. While the lithology is still fine-grained with limited bioturbation indicative of a marine setting, the increase in coarser grained deposits implies a more proximal position. This combined with the overlying deltaic facies indicates a prodelta depositional environment for this facies.

Delta Front Facies Association

Facies D1

Description

Facies D1 is composed of fine-grained sandstone with minor medium-grained sandstone (Fig. 6 B). The sandstone is interbedded with dark grey siltstone. The sandstone beds are more laterally continuous and more abundant

than in facies B2 (Fig. 6 B). The sandstone beds show sporadically distributed bioturbation ranging from BI 1-3 (Appendix 2, Fig. 7 A).

Interpretation

Facies D1 is interpreted as the deposits of a distal delta front. This is indicated by the increase in the proportion and bed thickness of sandstone within the facies in relation to facies B1 and B2. The thin nature of the sandstone beds compared to the thicker beds in facies D1 suggest deposition on the lowermost parts of the delta front; as the flows decelerated, they progressively deposited sand from suspension and tractional motion. The presence of ripple cross-lamination indicates periods of stronger unidirectional flow (Fig. 7 B). Other beds show swaley cross-bedding and interference ripples that indicate a combined-flow (wave and current) regime. The sporadically distributed bioturbation indicates periods conducive to opportunistic colonization, alternating with periods not favorable to invertebrate life. This is consistent with a subaqueous depositional environment affected by storms. The presence of fugichnia indicates periods of rapid deposition.

Facies D2

Description

Facies D2 is composed predominantly of amalgamated fine- to medium-grained sandstone with thin, rare, discontinuous dark grey siltstone beds. The sandstone bodies have erosional and soft-sediment-deformed bases and are arranged in crude coarsening-upwards cycles (Fig. 7 D). The thicknesses of sandstone bodies vary greatly over their lateral extent. Sandstone within this facies makes erosional contact with the underlying facies (Facies A3). The beds

show irregular bases with some isolated gutter casts. Dispersed throughout this facies are dark grey siltstone clasts. Bioturbation is rare, and where present, it is usually within the upper parts of sandstone beds that contain flat and low angle cross stratification. There is little if any bioturbation within the hummocky cross-stratified beds. The type of bioturbation present is not identifiable. This facies shows small quantities of highly comminuted plant debris (Fig. 11 E), which are distributed throughout the entire facies (Appendix 2).

Interpretation

Facies D2 is interpreted as the product of a proximal delta front. Based upon the increased abundance of sandstone relative to D1 indicating a more proximal location, together with the vertical context within coarsening-upwards sequences. The erosional base of facies D2 sandstones indicates that formative flows were powerful. The abundance of hummocky cross-stratification indicates a high energy, combined wave-current environment, possibly indicative of storm dominance. The influence of fluvial outflow can be discerned from the presence of current ripple cross-lamination and abundant, finely divided plant debris. The presence of siltstone clasts throughout indicates erosion of local substrates by powerful tractive currents. Finally, the lack of bioturbation in most beds is indicative of an environment that was not suitable for invertebrate organisms. This is compounded by the fact that what little bioturbation was present was probably destroyed by reworking.

Facies D3

Description

Facies D3 comprises fine grained sandstone that coarsens up to medium-grain sandstone (Fig. 6 B). The sandstone bodies are sharply-based, directly overlying facies D2. They are laterally extensive, extending across the entire study area. Compared to previous facies, there are fewer sedimentary features in D3; trough cross bedding is the dominant internal structure, together with flat and low-angle stratification. While most trough cross-sets (Fig. 7 C) show the modal flow direction towards the southeast, there are a small number of isolated beds that show an opposite flow direction towards the northwest (Fig. 8). The cross-bedding shows mud drapes, locally paired. In the lower parts of facies D3, sandstone bodies rarely preserve broken shell debris. There are some calcareous concretions in the lower parts of the beds. Beds rich in comminuted plant debris (Fig. 11 E) are distributed throughout facies D3. No bioturbation was observed in this facies (Appendix 2).

Interpretation

Facies D3 is interpreted as the deposits of mouth bars within a deltaic setting. Current-dominated environments are indicated by preserved sedimentary structures. The majority of the trough cross-sets indicate the downstream paleoflow direction at the river mouth (Fig. 8), while the trough cross-beds with opposed directions could reflect tidal inflow. This notion is supported by the presence of mud drapes within foresets. This sharp-based sandstone dominated by current-generated structures may indicate a friction-dominated mouth bar environment (Wright 1977). The broken shell fragments common near the base of

the facies could be an indication of a higher marine influence at the base. The rare bioturbation shows that the dynamic environment precluded any faunal colonization of the mouth bar except for isolated intervals. The presence of plant debris indicates fluvial outflow influence and the comminuted state of the plant material indicates an environment with the energy to break down all the land plant material.

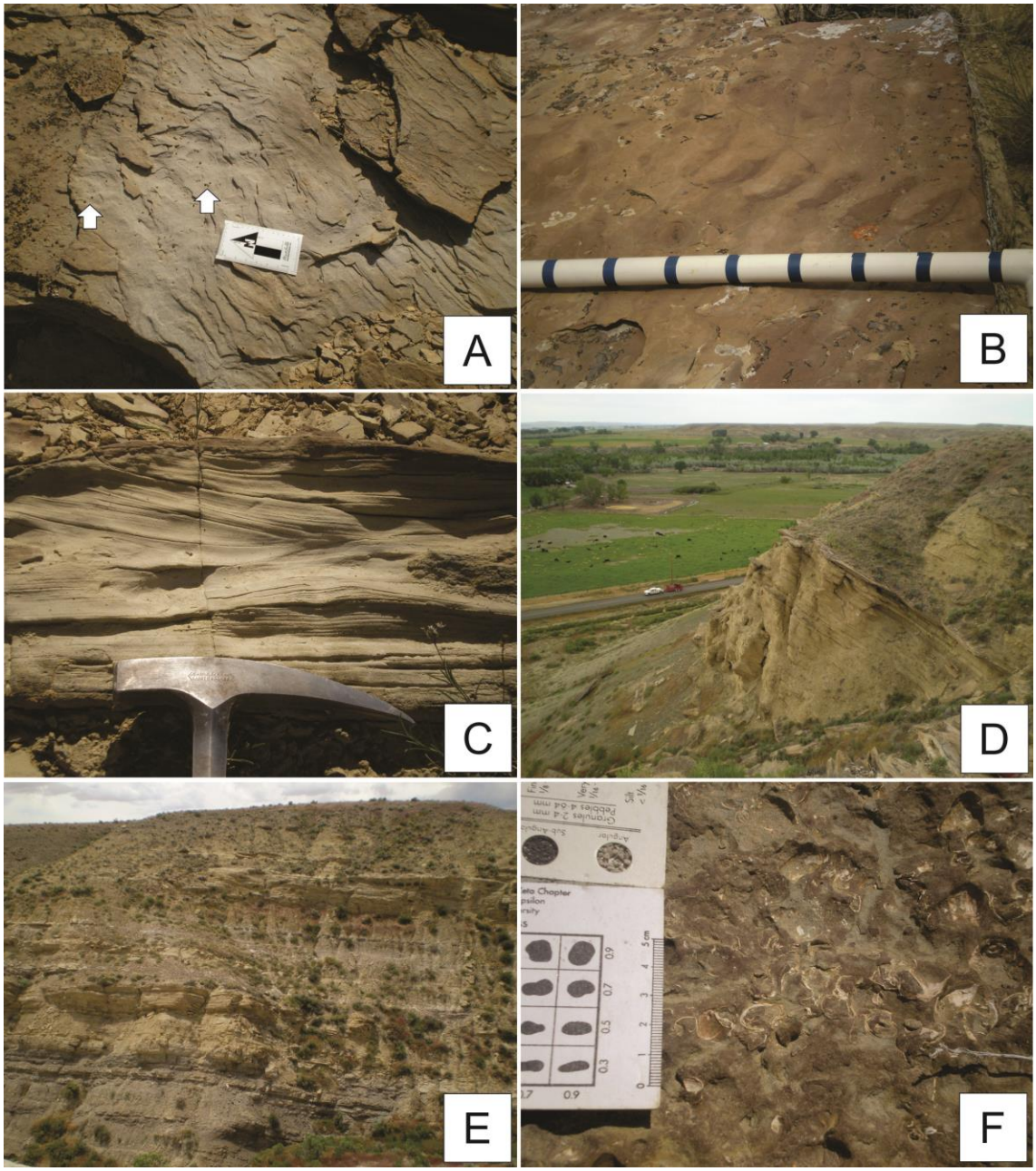

Figure 7: A. The paired openings of *Diplocraterion* as seen in both the distal delta front (facies D1) and incised estuary (facies I1) deposits. **B.** Asymmetrical ripples seen at the top layer of the distal and proximal delta facies (facies D1 and D2, respectively), indicating direction of paleocurrent flow. Jacob's staff for scale with 10 cm intervals marked. **C.** Small scale trough crossbedding present within the fine-grained sandstone of proximal delta front facies (facies D2) indicating the paleocurrent flow direction. **D.** One of the coarsening upwards units of the prodelta (facies B3) to distal delta front (facies D1) with lithologies ranging from siltstone to fine grained sandstone, indicating a proximal shift in deposition and a shallowing of the depositional setting. **E.** Lagoon deposits (facies C1) encased within coastal mire deposits (facies C3). The lagoonal deposits show a coarsening upwards trend then a fining upwards trend with coarse ripple laminated sandstone in the center of the section. **F.** Bed of broken brachiopod shells seen in the central lagoon facies (facies C1).

Coastal Platform Facies Associations

Facies C1

Description

Facies C1 is composed of thinly interbedded sandstone and dark grey to black siltstone (Fig. 6 C). Some rare shale partings are present locally. This facies varies greatly in thickness and bedding style throughout the study area. The percentage of sandstone to siltstone also varies considerably, with both coarsening and fining upwards trends preserved (Fig. 7 E); how well these trends are presented varies from north to south with the trends more apparent in the southern part of the study area. The sedimentary features present within the sandstone are symmetrical wave ripples and ripple cross-lamination. The top of the unit shows abundant bivalve shell debris in some cases (Fig. 7 F). There is very little bioturbation present; the BI is 0-1 (*Diplocraterion* is the only recognizable trace), but abundant plant rootlets and detrital plant debris are preserved (Appendix 3).

Interpretation

Facies C1 is interpreted as the product of a lagoonal environment on the basis of the thinly-interbedded lithology, together with evidence for terrestrial conditions (plant debris and *in situ* roots) and coastal conditions (bivalve shells). The mudstone present appears to have settled into the lagoon from suspension. The increased quantity of sand seen in the middle of facies intervals could reflect progradation of coastal systems into the formative lagoons. The symmetrical wave ripples and ripple cross-lamination indicate modest wave activity. The bivalve shells indicate a well oxygenated environment. The plant debris present is not as highly broken up as the plant debris in other areas, representing a lower-

energy environment and a shorter distance of transport. The presence of rootlets in the facies indicates periods of stasis during which plants were able to take root into the substrate. Facies C1 is predominantly found associated with facies C3.

Facies C2

Description

Facies C2 is composed of medium- to coarse-grained sandstone arranged in crude coarsening-upward sequences in some localities (Fig. 6 C). This facies is similar to facies D3 but is coarser-grained and comprises much thicker bodies up to 40 m thick. It also contains more siltstone clasts and siltstone partings than facies D3. Some intervals show local siltstone clast conglomerate beds that have been highly oxidized. This facies is dominated by trough cross-bedding and contains some macroform inclined bedding. This is a laterally extensive facies, present throughout the entire study area, but substantially increases in thickness towards the southern localities. Sporadic bioturbation occurs throughout with a BI of 0-1. Finally, there are local zones that show pedogenic alteration (Appendix 3). The paleocurrent directions from this facies indicate a predominantly southeasterly flow direction with some beds showing bipolar flow distribution with a northwestern flow direction (Fig. 8).

Interpretation

Facies C2 is interpreted as the deposits of coastal distributary channels. The dominance of medium- to coarse-grained sandstone indicates powerful tractional flows capable of carrying coarse sediment. The dominance of trough cross-bedding indicates that the facies was formed by uni-directional flows. Some isolated beds show bi-directional cross-bedding with mud drapes, suggesting tidal

backflow (Fig. 8). The dominant paleoflow direction from this facies is to the southeast, indicating the regional direction of sediment dispersal. The presence of internal erosion surfaces indicates that some facies C2 bodies are amalgamated, multistory bodies. The presence of local comminuted plant debris (Fig. 11 E) indicates that breakdown of terrestrial plants contributed to the sediment budget. Finally, pedogenic alteration is seen in some beds that indicates periods of sub-aerial exposure. While some of the interpretation is similar to the proximal delta front, the decrease in fine grained deposits, combined with the relationship this facies has with the more terrestrial facies, such as the coastal mire and lagoon, indicate a more terrestrial environment of deposition. This interpretation is supported by the increase in plant debris that would be more common in a terrestrial environment.

Facies C3

Description

The lithology in facies C3 ranges from dark grey siltstone, through carbonaceous shale, to coal (Fig. 6 C). Plant debris and rootlets are abundant. While coal is present in this facies throughout the entire study area, no one bed of coal is traceable throughout the study area. Coal beds are mostly less than 1 m thick. This facies is found sharply overlying facies D2 and is commonly erosionally overlain by facies C2 (Appendix 3).

Interpretation

Facies C3 is interpreted as the deposits of coastal mires formed on a waterlogged coastal plain. The presence of coal and rootlets indicates that vegetation was able to colonize abandoned portions of the coastal plain indicative

of a wetland environment that was stable for long stretches of time. The compositional layering with some siltstone lenses indicates periodic flooding events that introduced silt into the wetland system.

Incised Estuary Facies Association

Facies I1

Description

The lithology in facies I1 is composed of fine- to medium-grained sandstone with sporadic thin siltstone partings (Fig. 6 D). There is a wide range of sedimentary features including ripple cross-lamination, interference ripples, symmetrical wave ripples and small-scale trough cross-bedding (bi-modal). This facies has a sharply erosional base. The sandstone beds show sporadically distributed bioturbation ranging from BI 1-3. Highly fragmented shell debris is found sporadically within some beds, but is uncommon. Sporadic plant debris is present in trough cross-beds (Appendix 4).

Interpretation

Facies I1 is interpreted as the deposits of an incised estuary. The erosional base of facies I1's sandstones indicates that formative flows were powerful. This overlies fine-grained deposits of facies B2. The sandstone shows beds with abundant trough cross-bedding with associated highly broken up plant debris indicative of fluvial input into the environment. Other beds show features of combined flow, such as symmetrical wave ripples and interference ripples, and the combined flow-dominated beds are associated with an increased abundance of bioturbation and broken shell fragments. This indicates periods of increased marine influence. The sharp base of this facies and its position in relation to the

finer-grained offshore facies (facies B2) combined with the interrelation of fluvial and marine indicators argue for an incised estuarine environment where fluvial and tidal forces were balanced.

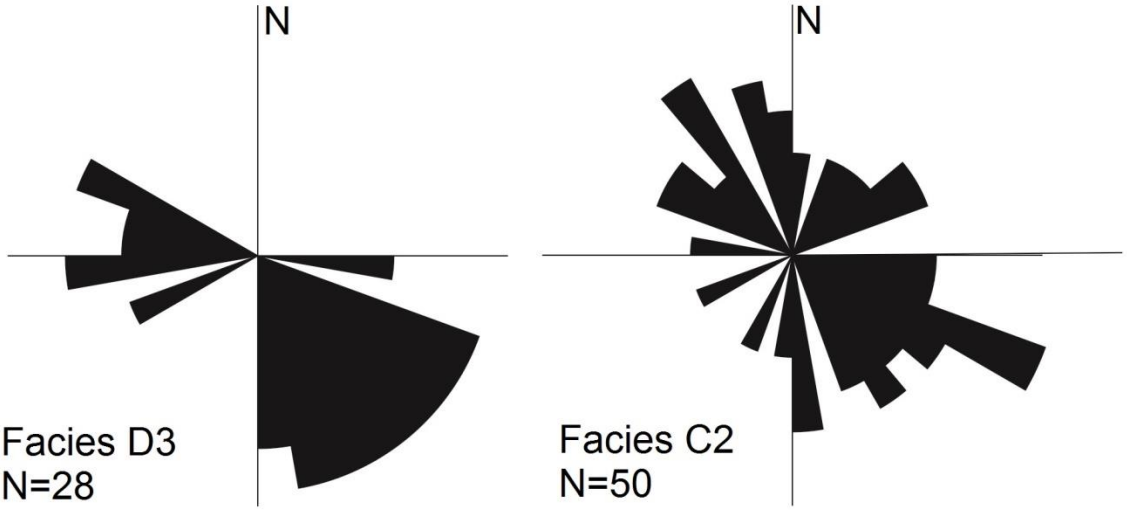

Figure 8: Rose diagrams showing the pattern of sediment dispersal for facies D3 (mouth bar) and facies C2 (distributary channel). Both show a bi-modal distribution with the dominant direction to the SE and a secondary distribution to the NW.

Lithostratigraphy

The facies stacking patterns in the Mesaverde Group show a dominance of deltaic and fluvial facies throughout. While deltaic facies become more common upward in the unit, they are present throughout. Many contacts between the formations are sharply based, with little or no gradation between individual formations (Fig. 9).

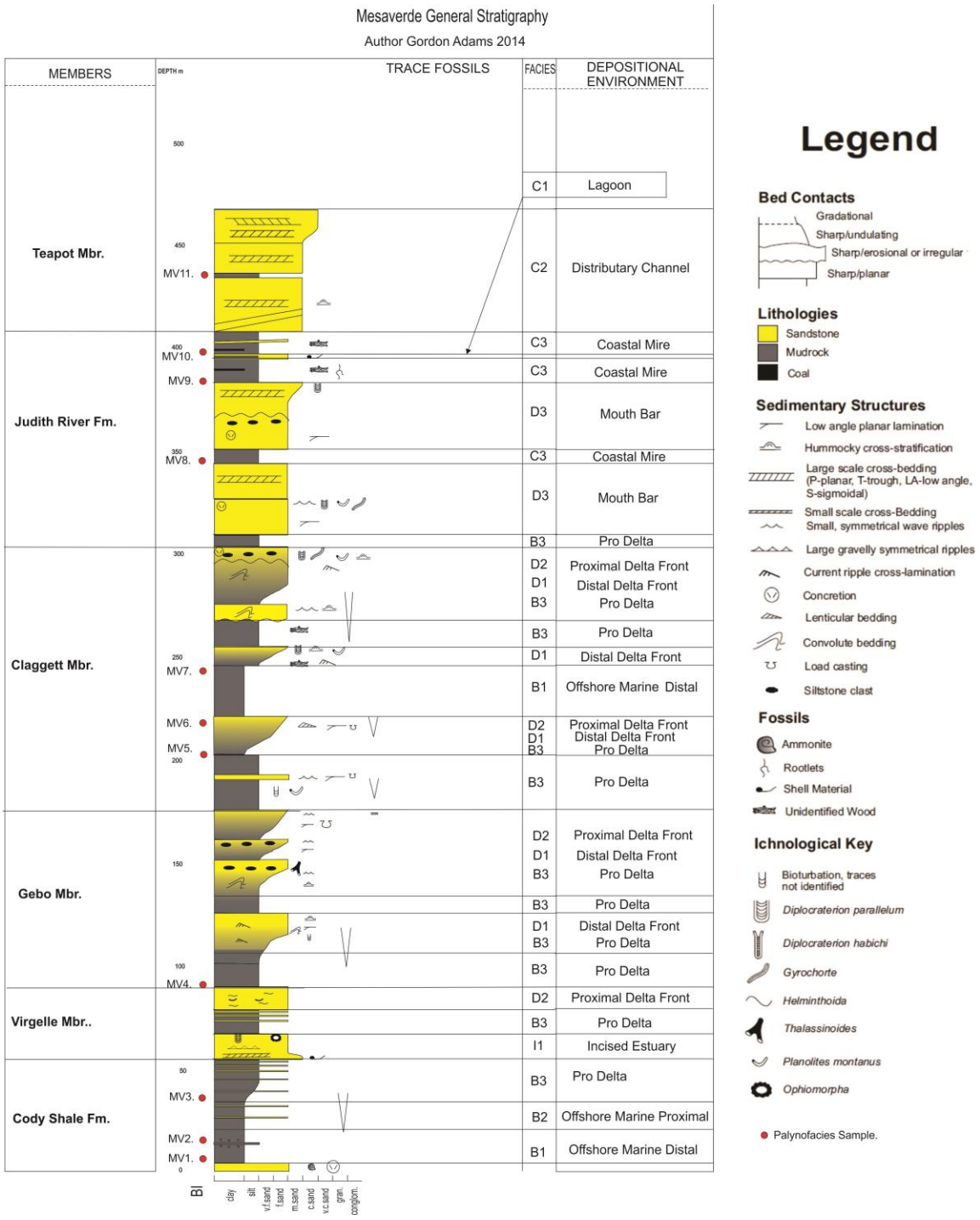

Figure 9: Lithostratigraphy of the Mesaverde Group in the study area. This is a composite section created from localities 1 – 5.

Unit Name	Thickness	Facies Present	Stacking Patterns	Lateral Variations
Cody Shale	Unknown	Facies B1 (Distal offshore marine) & B2 (proximal offshore marine to lower shore face)	Facies B1 passes gradationally into B2.	Minor lateral variation in presence of bentonite beds.
Virgelle Mbr.	Up to 20 m	Facies I1 (incised estuary), B3 (prodelta) & D1 (distal delta front)	Facies I1 sharply overlies the Cody Shale. This is then sharply overlain by facies B3 that passes gradationally in to facies D1.	Thins towards the southeast. Sandstone bed thickness decreases & sedimentary structures become less well represented.
Gebo Mbr.	Up to 94 m	Facies B3 (prodelta), D1 (distal delta front) & D2 (proximal delta front)	Facies B3 sharply overlies both the Virgelle Mbr. and facies D1. Facies D1 gradationally overlies facies B3. Facies D2 transitionally overlies facies B3 and is arranged in a number of coarsening upwards sequences. Sequence thickness ranges between 5 - 10 m.	Thins towards southeast. Sandstone bodies become more amalgamated and sedimentary structures are increasingly poorly represented.
Claggett Shale Mbr.	Up to 135 m	Facies B1 (Distal offshore marine), B3 (prodelta), D1 (distal delta front) & D2 (proximal delta front)	Facies B3 sharply overlies the Gebo Mbr. This then fines upwards into facies B1. Facies B1 is then overlain transitionally by facies D1. Facies D1 is then sharply overlain by facies B3. Facies D2 erosively overlays facies B3 and is arranged in a coarsening upwards sequence.	More sandstone rich in the central part of the study area than in the north or the south. Thins towards the center of the section.
Judith River Fm.	Up to 118 m	Facies B3 (prodelta), facies D3 (mouth bar), facies C1 (lagoon) & facies C3 (coastal mire)	Facies B3 sharply overlies the Claggett Mbr. This is then sharply overlain by facies D3. Facies D3 is a thick unit that coarsens upwards toward the stratigraphic top of the unit. Facies C3 sharply overlies facies D3. Facies C1 is present within facies C3 and shows both coarsening and fining upwards trends.	Thins towards the southeast. Shale facies thin and become more amalgamated towards the southeast. Lagoon facies poorly preserved in the northwest.
Teapot Sandstone Mbr.	Up to 85 m	Facies C2 (coastal distributary channel)	Facies C2 sharply overlies the Judith River Fm. It has thick sandstone beds 10 - 20 m. It coarsens upwards towards the stratigraphic top of the section.	Thickens towards the northwest of the section.

Table 1: Members of the Mesaverde Group and the facies that compose them. Fm stands for formation, Mbr stands for member.

The lithologies in each component member identified in this study (Table 1) and their stacking patterns are consistent with previous studies (Condon 2000; Swift et al. 2008; Martinsen et al. 1993). However, the interpretation of these lithologies is not consistent with all previous studies. While the dominance of deltaic and fluvial facies is consistent with Swift et al. (2008) and Martinsen et al. (1993), it contrasts with the depositional interpretation of Condon (2000) who interpreted the Mesaverde Group as recording a transition from offshore marine to coastal deposits with no reference to deltaic systems. This may be due to numerous reasons. The first is poor exposure or preservation of sedimentary structures of the respective study areas. Another possible explanation is that these studies may not have conducted a full lithofacies analysis leaving a more general interpretation of the depositional environment as simply marine and non-marine (Fig. 10). The contacts between formations in this study are also different from previous studies. In the present study area, stratigraphic contacts show little to no gradation between formations. Previous studies by Condon (2000) and Severn (1961) both show gradational contacts between the Cody Shale and the Eagle Formation and the Claggett Member and the Judith River Formation. This could be due to either the paleogeographic location of deposition; the studies by Severn (1961) and Condon (2000) being in a more proximal area with greater terrestrial input and lesser marine input recording a more gradational relationship with the sandstone increasing overtime. The more distal studies areas, such as this study and Fitzsimmons and Johnson (2000), with a greater marine influence preserve sandstone bodies with sharper bases. The other potential explanation could be related to the vagaries of exposure (Figs. 9 & 10).

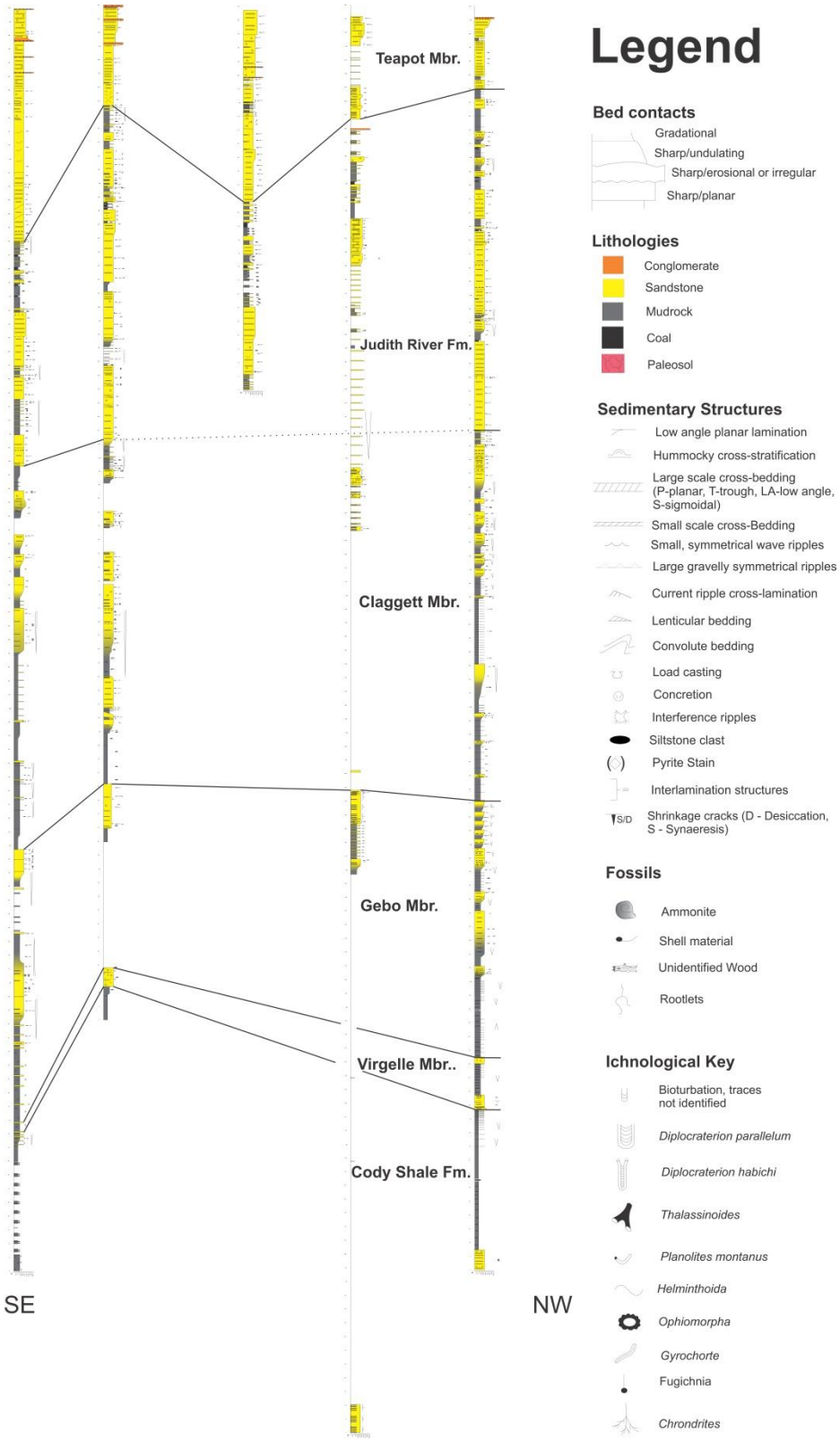

Figure 10: Logged section from the Bighorn Basin divided up into members using key facies changes throughout the section. A shift to a more proximal depositional environment can be seen both vertically throughout the section and also to the south of the section.

Palynofacies Assemblages

The samples used for palynofacies analysis where taken from fine-grained lithologies throughout measured section 1 (Figs. 4 & 9). The facies represented in the analysis are distal offshore marine (B1), prodelta (B3), coastal mire (C3) and distributary channel (C2). A 300 sample point count was conducted on each sample (Table 3), and then the palynofacies were investigated using four different methods of quantitative analysis: principal components analysis, cluster analysis, factor analysis and the Tyson Ternary Diagram.

The palynodebris types used in the counts are listed in table 2. The palynomorphs range from marine indicators such as marine palynomorphs and Amorphous Organic Matter (AOM) to terrestrial indicators such as sporomorphs and phytoclasts (Fig. 11). The range of phytoclasts present, from structured to comminuted, represent the breakdown of phytoclasts through mechanical and chemical means, indicating factors such as distance transported and energy in the environment. While the palynomorphs described in table 2 are used as environmental indicators, the presence or absence of one of the palynomorphs is not enough to identify the depositional environment. It is the overall composition and ratios of the palynomorphs that is considered in determining the depositional environment. The most commonly seen palynomorphs in this study are AOM, opaques, structures phytoclasts and comminuted phytoclasts (Fig. 11)

Palynomorphs / organic debris	Descriptions
Sporomorphs	Embryophytic spores and pollen grains derived from land plants
Fungal remains	Dark brown spores, filamentous hyphae, and mycelia (fruiting bodies of fungal origin)
Freshwater algae	Mostly Pediastrum and Azolla spores with massulae, and rare specimens of Botryococcus
Marine palynomorphs	Dinoflagellate cysts, acritarchs, and chitinous inner linings of foraminifera
Structured phytoclasts	Structured remains of land plants, including lath-shaped or blocky wood particles, parenchyma, and thin cuticle fragments. With the exception of black debris (described below), fragments with some form of cellular structure or definite shape are included in this category
Unstructured phytoclasts	This category included highly degraded plant remains without much structure with colors ranging from yellow to dark brown and nearly black, comminuted brown debris with sizes <5 lm, and amber-colored, globular to angular particles of resin
Black debris	Most particles are opaque and often have shapes similar to wood, although some are rounded and appear to be highly oxidized palynomorphs
Amorphous organic matter	Fluffy, clotted and granular masses with colors ranging from almost colorless to yellow and pale brown. This category is marine in origin, and formed as a result of degradation of algal matter

Table 2: Table of palynomorphs used in palynofacies analysis.

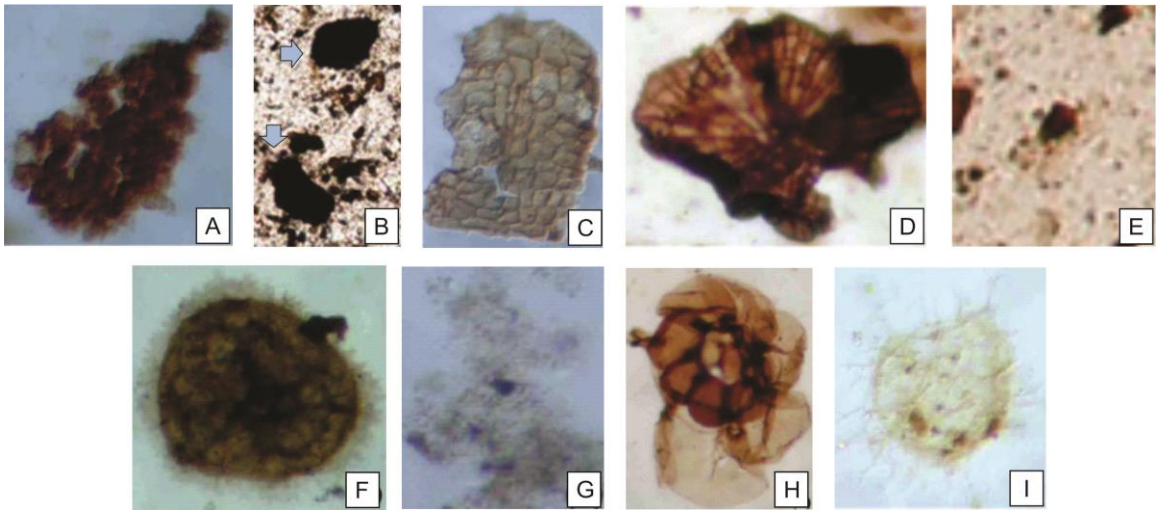

Figure 11: Example images of palynomorphs used in identification in this study. Modified from Oboh-Ikuenobe (2005). **A:** Degraded phytoclast. **B:** Opaque, also known as black debris, indicated by arrows. **C:** Structured phytoclast. **D:** Fungal remains. **E:** Comminuted phytoclast. **F:** Pollen/spore. **G:** Amorphous organic matter, also known as AOM. **H:** Fresh water algae. **I:** Dinoflagellate cyst.

Sample	Comminuted	Degraded	Opaque	Structured	Fungal	Pollen/Spores	AOM	Non Marine Algae	Fresh Water Algae	Dino Cyst	Total
MV1	206	3	30	4	0	11	44	0	0	2	300
MV2	213	2	32	0	0	10	43	0	0	0	300
MV3	221	1	48	3	0	9	18	0	0	0	300
MV4	187	27	51	21	0	5	9	0	0	0	300
MV5	195	26	34	39	0	6	0	0	0	0	300
MV6	166	13	23	78	0	20	0	0	0	0	300
MV7	200	12	11	60	2	12	3	0	0	0	300
MV8	146	9	2	122	1	20	0	0	0	0	300
MV9	188	17	0	87	0	8	0	0	0	0	300
MV10	252	1	2	15	0	3	26	0	0	1	300
MV11	232	1	0	12	0	2	53	0	0	0	300

Table 3: Sample counts from this study used in palynofacies analysis.

Principal Components Analysis

Principal components analysis is a "projection of a multivariate data set down to as few dimensions (principal components) as possible in a way that preserves as much variance as possible" (Hammer and Harper 2006). These dimensions can then be interpreted using the environmental affinities of the end members and weighted members of the assemblage. The results from a principal components analysis are usually displayed using a scatter diagram. This plots each sample using a coordinate system in which the two dominant components represent an axis with both positive and negative coordinates. Positive coordinates represent one end member of the component and the negative represents the other (Hammer 2014). This allows samples to be grouped by similarity.

The principal components analysis conducted on the palynomorph counts of this study show two principal components that explain a large enough portion of the variance to be statistically significant. These are called principal components one and two. Principal component one explained 76.5% of the variance and principal component two explained 15.9% of the variance (Fig. 12). While there are five other components, they do not explain enough of the variance to be statistically significant. Principal component one's two end members are comminuted phytoclasts and structured phytoclasts (Appendix 5). There is a relationship between the two end members, wherein one increases as the other decreases. Secondary members including Amorphous Organic Matter (AOM; Fig. 15 A) seem to also show a relationship with comminuted phytoclasts (Fig. 15 E) and structured phytoclasts (Fig. 15 B). AOM is more common where there are abundant comminuted phytoclasts, whereas pollen and spores are more abundant where

there are abundant structured phytoclasts (Fig. 11). Principal component two (Appendix 6) indicates two end members which are black debris (opaques) and phytoclasts. The abundance of black debris (Fig. 15 A) appears to increase as the abundance of most other groups decreases.

On a scatter diagram (Fig. 12), the structured phytoclasts end member is represented by the negative coordinates and the comminuted phytoclasts end member is represented by the positive coordinates. For principal component two, the end member defined by amount of opaques (Fig. 11 B), is represented by negative coordinates and the end member defined by phytoclasts is represented by the positive coordinates. Four groupings are evident (Fig. 12). Group one consists of samples MV7 and MV9. Group two consists of samples MV5 and MV6. Group three consists of samples MV10 and MV11. Group four consists of samples MV1, MV2, MV3 and MV4. Sample MV8 is an outlier that does not fit within any of the groups (for sample lithology and position within the Mesaverde Group see Fig. 9).

Group one plots negatively for principal component one and positively for principle component two, indicating a high abundance of structured phytoclasts and spores/pollen and low abundance of black debris (Fig. 11). Group two plots negatively for both principal components one and two. This is an indication of a high abundance of structured phytoclasts and spores/pollen and a high abundance of opaques. Group three plots positively for both principal component one and two. This indicates a high abundance of comminuted phytoclasts and AOM and low abundances of opaques. Finally, group four plots positively in principal component one and negatively in

principal component two. This indicates a high abundance of comminuted phytoclasts, AOM and opaques.

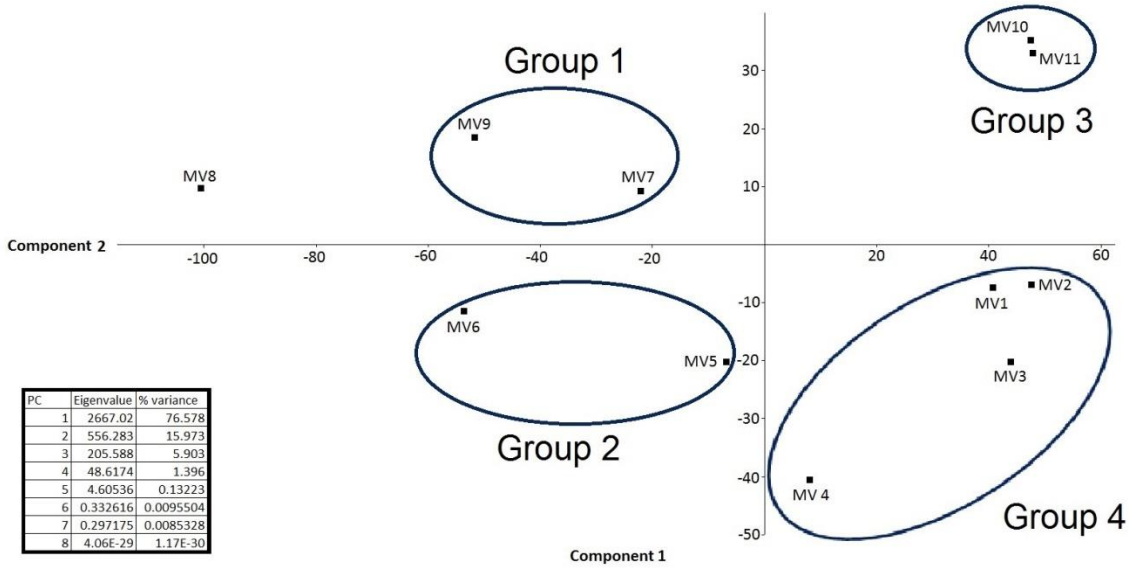

PC	Eigenvalue	% variance
1	2667.02	76.578
2	556.283	15.973
3	205.588	5.903
4	48.6174	1.396
5	4.60536	0.13223
6	0.332616	0.0095504
7	0.297175	0.0085328
8	4.06E-29	1.17E-30

Figure 12: Scatter graph of principal components analysis. Component one is interpreted as a change from comminuted to structured phytoclasts. Component two is interpreted as the amount of opaques in samples.

Factor Analysis

The third method of analysis is CABFAC (*Ca*lgary and *B*rown *Fac*tor Analysis) factor analysis (Klovan and Imbrie 1971). This method of analysis uses a varimax rotation on row normalized data (Hammer 2014) to maximize the correlation of the data. This is done by rotating the samples in multidimensional space to find the highest factor of correlation. This analysis shows only one principal component that explains a significant percentage of the variance (Fig. 13). This factor is defined by the relationship between comminuted phytoclasts and AOM on one side of the axis and structured phytoclasts on the other (Fig. 13). The samples split into two groups and an outlier. The first group in the plot is composed of samples MV4, MV5, MV6, MV7 and MV9, which have the highest amount of structured phytoclasts. The other group is composed of samples MV1

MV2, MV3, MV10 and MV11, which show an abundance of comminuted phytoclasts and AOM (Fig. 14). The arrangement of these two groups and outlier show a gradient ranging from MV8 to MV2. The side of the gradient with MV8 is represented by low amounts of AOM and comminuted phytoclasts and high amounts of structured phytoclasts and an increase in pollen and spores (Fig. 11). The opposite side of the gradient shows high AOM and comminuted phytoclasts and low structured phytoclasts and spores.

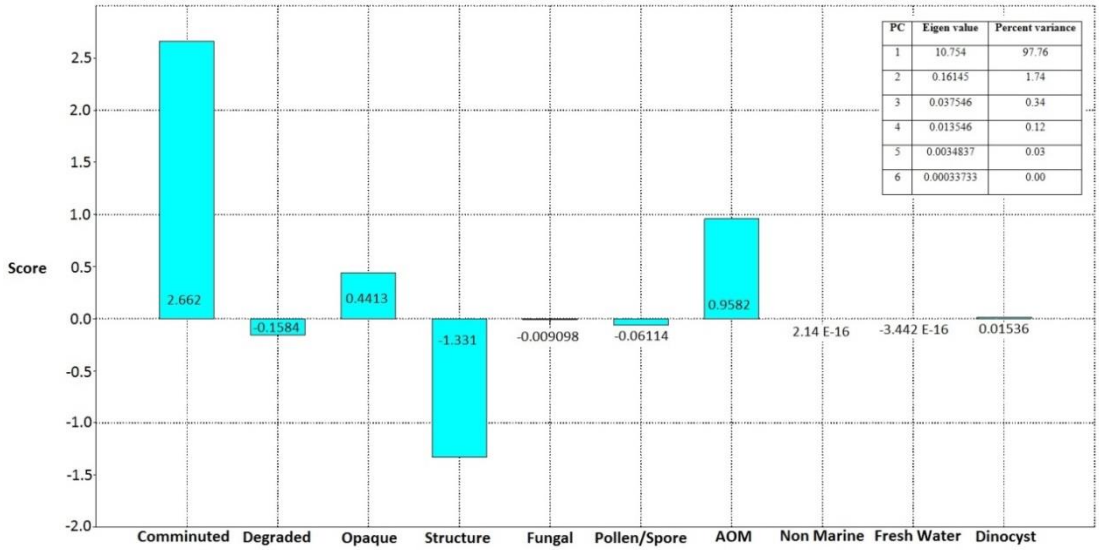

PC	Eigen value	Percent variance
1	10.754	97.76
2	0.16145	1.74
3	0.037546	0.34
4	0.013546	0.12
5	0.0034837	0.03
6	0.00033733	0.00

Figure 13: This chart shows the weighting of the different groups within the factor analysis that control the distribution of samples in the factor analysis. With CABFAC principal components Eigen value table.

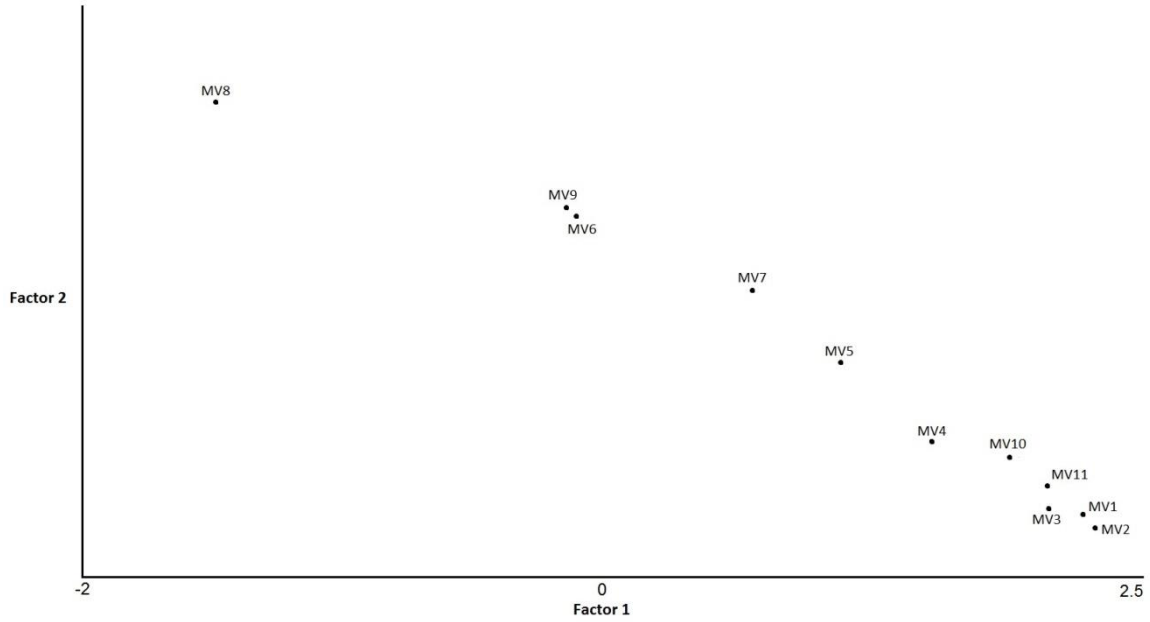

Figure 14: This chart show the samples from the Mesaverde Group plotted against the factors from the factor analysis. Factor two is not a statistically viable factor; only factor one has relevance. The spread of factor one from right to left indicated a variance of marine and terrestrial input into the system. The right side of the chart show higher amounts of AOM and comminuted phytoclasts which indicated a distal environment. The left side of the chart has more structured phytoclasts and indicate a more proximal environment. Two groups are identifiable with MV8 as an outlier.

Tyson Ternary Analysis

The final analysis entailed plotting the data on a Tyson Ternary Diagram (Tyson 1993). The Tyson Ternary Diagram does not use all the different groups that have been used for the previous analyses, but focuses on total phytoclasts, palynomorphs and AOM. While there are two groupings of samples, all samples are classified as having affinities with proximal settings subject to high terrestrial influx. The plotted Tyson Ternary Diagram is superimposed over the ternary field scheme; the two different groups fall into different parts of the scheme. The first grouping falls under ternary field two which represents marginal, dysoxic to anoxic basin environments. The other grouping falls under ternary field one, which represents proximal shelf or basin environments. All these samples correspond to a type three gas-prone kerogen type (Fig. 16). The positioning of all

the samples in the ternary diagram also indicates a high terrestrial and fresh water influx to the system because even where there is an abundance of marine indicators, there is also evidence for terrestrial materials.

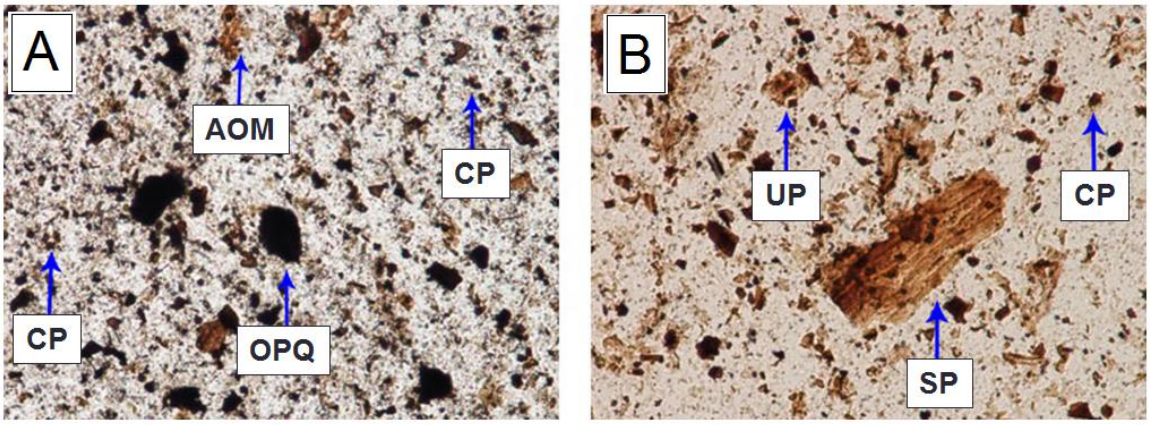

Figure15: A: MV2 from distal offshore marine deposit at the base of locality one (Fig. 9); contains an abundance of AOM, comminuted phytoclasts (CP) and opaques (OPQ); interpreted as indicating a distal environment. **B:** MV7 from the base of distal delta front deposit in the center of locality one (Fig. 9) with abundant structured (SP) and unstructured phytoclasts (UP) interpreted as reflecting a more proximal environment.

All of the analyses produced similar groupings; the cluster analysis and the principal components analysis exhibited a second grouping involving opaques that was not present in the other methods. The change in the abundance of opaques seems to correspond to where the samples were taken from in the Mesaverde Group rather than with changes in the other palynodebris. This could indicate a temporal rather than environmental factor. Therefore the terrestrial components of the samples were plotted on a graph to determine whether the presence of opaques is a temporal or environmental factor (Appendix 7). The diagram shows that while all the other samples seem to change in amounts in relation to one another over time, the black debris seems to decrease with little relation to the other groups present. This can be interpreted as a response to an

external factor such as increased fire activity rather than environmental changes related to paleobathymetry.

Initial Environmental Interpretations

The initial environmental inferences from the palynofacies analysis, before they are viewed in conjunction with the lithofacies analysis, indicate a gradient from MV8 to MV2. When this gradient is plotted in order of the samples, there is a decrease in distal indicators such as AOM and comminuted phytoclasts over the gradient and an increase in structured phytoclasts and spores (Fig. 11 C & F), both used as proximal indicators (Appendix 8). The gradient seen predominantly indicates a more proximal environment of deposition vertically throughout the section, with the exception of MV10 and MV11 (Fig. 18). The principal components analysis produced four groupings but due to the fact that one of the groupings was defined by the presence of opaques (Fig. 15), it is believed to be a temporal feature; two groups can be recognized based on their depositional environmental affinities. The first group is composed of MV1, MV2, MV3, MV4, MV10 and MV11, and is defined by high amounts of distal indicators; the second group is composed of MV5, MV6, MV7, MV8 and MV9 (Figs.12 & 14) and is defined by high amounts of proximal indicators. These groupings show a more proximal environment of deposition vertically throughout the system, with the exception of samples MV10 and MV11. The more distal grouping contains the samples lower in the measured section and the proximal grouping contains samples higher vertically in the section.

The Tyson Ternary Analysis indicates that the samples span two environmental groupings: group one from marginal, dysoxic to anoxic basin environments and group two from proximal shelf or basin environments. Group one has a large portion of comminuted phytoclasts and AOM (Fig. 11 E & G). The comminuted phytoclasts indicate a process under which land plant material is broken down either by transportation from the shoreline or a chemical process (Batten 1996). The AOM, while it can be formed in lacustrine environments, is known to be primarily a marine indicator. The combination of these factors indicates that group one has a higher marine influence than group two. Group two has less comminuted phytoclasts and very little AOM, in some cases none. Group two samples also seem to have an abundance of structured phytoclasts and an increased amount of pollen and spores (Fig. 11 C & F). The increased abundance of pollen and spores indicates an environment that is more proximal, with a higher clastic input. This would explain the structured phytoclasts, because more proximal phytoclasts would not have had as long to degrade as those in a more distal setting. While both groups seem to be from a near shore marine setting, the variation between the groups appears to be due to marine influence and distance from the coast. A more in-depth environmental analysis that combines these findings with the facies analysis will be discussed below.

The abundance of phytoclasts in all palynofacies samples from the study area could be due to one of two environmental factors. The first is that all the samples came from an area of high oxidation such as a fluvial or delta top setting. In settings like these, the highly resistant nature of the lignin present within the

phytoclasts led to the phytoclasts being the dominant preserved organic material. The second environmental factor is transportation distance. The resistant nature of the lignin allows for the phytoclasts to be preserved through travelling a greater distance to deposition. This longer transportation distance leads to a decrease in the abundance of structured phytoclasts and an increase in the abundance of comminuted phytoclasts (Fig. 11 E) (Tyson 1993). For this study, both environmental factors would likely have contributed to the abundance of phytoclasts within the system.

Finally, the arrangement in the Tyson Ternary Diagram (Fig. 16) is similar to what has been seen in previously studied deltaic deposits using this method. The arrangement of points is similar to data from the Middle Jurassic deltaic Brent Equivalent in well 25/4-1 from the Norwegian North Sea (Tyson 1993). The results of the Tyson Ternary analysis combined with the findings of the other palynofacies analysis indicates a deltaic environment with a distal to proximal facies change vertically through the measured sections with some variation at the top of the Mesaverde Group. Samples MV10 and MV11 do not follow the proximal shift pattern seen in the other samples from the Mesaverde Group. Instead of a proximal shift seen in the rest of the section, a more distal environment is shown in the upper Judith River Formation and the Teapot Member. One of the most plausible reasons for this shift is that the fine grained material the samples were retrieved from could preserve a short-lived marine flooding event with an increase in tidal influence in the section. Another reason could be poor preservation within these samples; this is unlikely, however, as the sample in question still shows a

good variety and abundance of palynomorphs that would not be seen in a sample with poor preservation.

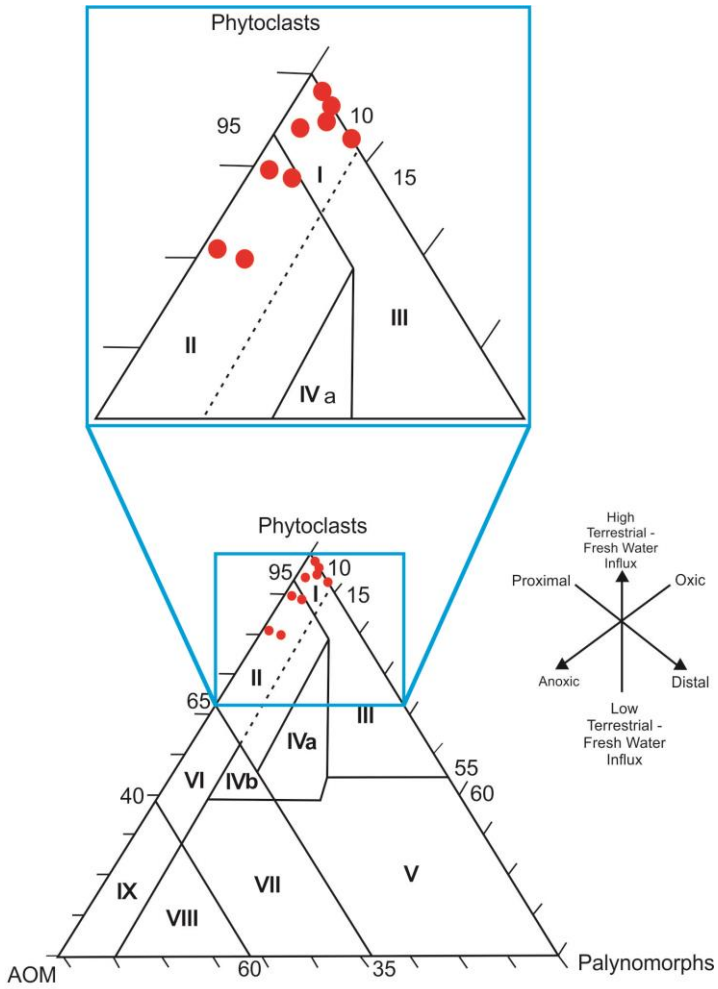

Ternary Field	Kerogen Type	Environment
I	III, gas prone	Proximal shelf or basin
II	III, gas prone	Marginal, dysoxic - anoxic basin
III	III or IV, gas prone	Proximal shelf
IV	III or II, gas prone	Shelf to basin transition
V	III > IV, gas prone	Mud dominated, oxic shelf
VI	II, oil prone	Proximal, suboxic - anoxic shelf
VII	II, oil prone	Distal, dysoxic - anoxic shelf
VIII	II >> I, oil prone	Distal, dysoxic - oxic shelf
XI	II > I, highly oil prone	Distal, suboxic - anoxic basin

Figure 16: Tyson Ternary Diagram of samples in this section placed within a ternary field diagram representing both the environment and kerogen type of the samples. Chart modified from Tyson (1993).

Synthesis and Depositional Environment

Synthesis of Lithofacies and Palynofacies

The lithofacies stacking patterns present within the Mesaverde Group show a distal to proximal depositional environment change through the entire vertical succession. Facies present change from dominantly basinal to through to coastal platform facies. The most common facies association seen in the Mesaverde Group is the delta front facies association. It is a dominant facies that is present in the Eagle Formation, the Gebo Member, the Claggett Member and the Judith River Formation (Fig. 8).

The palynofacies also show a distal to proximal depositional environment change vertically through the Mesaverde Group (with the exception of samples MV10 and MV11). The final palynofacies samples MV10 and MV11 show a more distal environment of deposition that is not seen in the lithologies and sedimentary structures of that part of the Mesaverde Formation. The possible reasons for this shift were discussed in the palynofacies section. The heightened distal influence seen in the palynofacies does not correspond with the lithofacies representing MV10, facies C3 (coastal mire) or MV11, from facies C2 (distributary channel), both representing some of the more proximal environments in the Mesaverde Group. The reason the distal facies within this group were not identified is most likely due to the poor quality of the outcrop. This would show that while there is an overall distal to proximal shift vertically throughout the section, there were small scale flooding events that were not exposed in the outcrop due to this part of the measured section being covered in soil and debris, but are identifiable through palynofacies analysis (Fig. 12).

The proportion of the palynological samples that is made up of distal and marine indicators such as AOM decreases vertically throughout the Mesaverde Group, while proximal and terrestrial indicators such as structured phytoclasts (Fig. 11 C & G) increase. The distribution of the palynofacies samples also indicates a deltaic environment when plotted on the Tyson Ternary Diagram (Fig. 16). Therefore both the palynofacies and lithofacies indicate a dominantly deltaic environment with an overall shift from distal to proximal depositional environment throughout the vertical succession of the Mesaverde Group.

Sequence Stratigraphy

Sequence stratigraphy analyzes the sedimentary response to cycles of base level change, and the depositional trends that emerge from the interplay of accommodation and sedimentation (Catuneanu 2006). Sequence stratigraphy divides a lithological section into genetically related sequences divided by sequence boundaries, which are erosional discontinuities caused by relative drawdown of sea level. Sequence boundaries are indicated by an abrupt shallowing of facies within the section represented by an abrupt proximal facies shift and a corresponding erosion surface. This is overlain by a lowstand systems tract represented by the coarsest sediments in the system and which tends to have a progradational to slightly aggradational profile. The next part of the sequence is the transgressive systems tract representing base level rise and is capped by the maximum flooding surface. The transgressive systems tract is identified by a fining upwards of sediments and a retrogradational stacking pattern, representing a distal shift in the depositional setting of the system up to the maximum flooding surface (MFS). The MFS represents the most landward position of the shoreline, and will usually be the finest-

grained and most distal facies in the sequence. Above the MFS is the highstand systems tract. This represents the later stages of base level rise when sedimentation rates are higher than base level rise allowing for progradation of proximal facies into a marine environment. The highstand systems tract is usually represented by one or more coarsening upwards sequence (parasequence), and an aggradational to progradational stacking pattern (Catuneanu 2006).

The sequence stratigraphy of the Mesaverde Group has been examined by numerous researchers (Martinsen et al. 1995, Mellere & Steel 1995, Fitzsimmons & Johnson 2000, Swift et al. 2008, Kieft et al. 2011), but not in the northern or central Bighorn Basin. Previous studies in the basin have focused only on the outcrops around the western and southern rim of the Bighorn Basin (Fitzsimmons & Johnson 2000; Swift et al. 2008). This study focuses on the sequence stratigraphy in the northern Bighorn Basin in Wyoming to allow a more regional view of stratal stacking patterns. Within the Mesaverde Group, four sequences have been defined, both in previous studies, and in the present work: the Fishtooth Sequence, the Gebo Sequence, the Judith River Sequence and the Teapot Sequence, from base to top. The names of the sequences are derived from standard stratigraphic nomenclature for the region (Fig. 18 & Fig. 17).

The Fishtooth Sequence is poorly exposed throughout the studied region. The base is only present in measured section two. The Fishtooth Sequence as a whole is only exposed within localities one, two and four and is not fully exposed at these localities, so information on this sequence is limited. The base of the Fishtooth Sequence is a sharp-based sandstone unit that overlies shale of offshore marine shelf origin. The rest of the sequence is so poorly exposed that the systems tracts are difficult to interpret. Where the

sequence is well-exposed, there is an upward transition to finer-grained deposits representing offshore marine and prodelta deposits. These facies transitions indicate a period of increasing formative water depth. Above this, the change to prodelta deposits indicates shallowing. The change to finer grained deposits and interpreted increasing water depth is compatible with a transgressive systems tract where the increase in sea level outpaces the sediment supply. The coarsening upwards at the top of the Fishtooth Sequence is comparable to a highstand systems tract in which sediment supply overtakes the rate of sea level rise. This results in the more terrestrial-influenced facies seen towards the top of the Fishtooth sequence (Figs. 17 & 18).

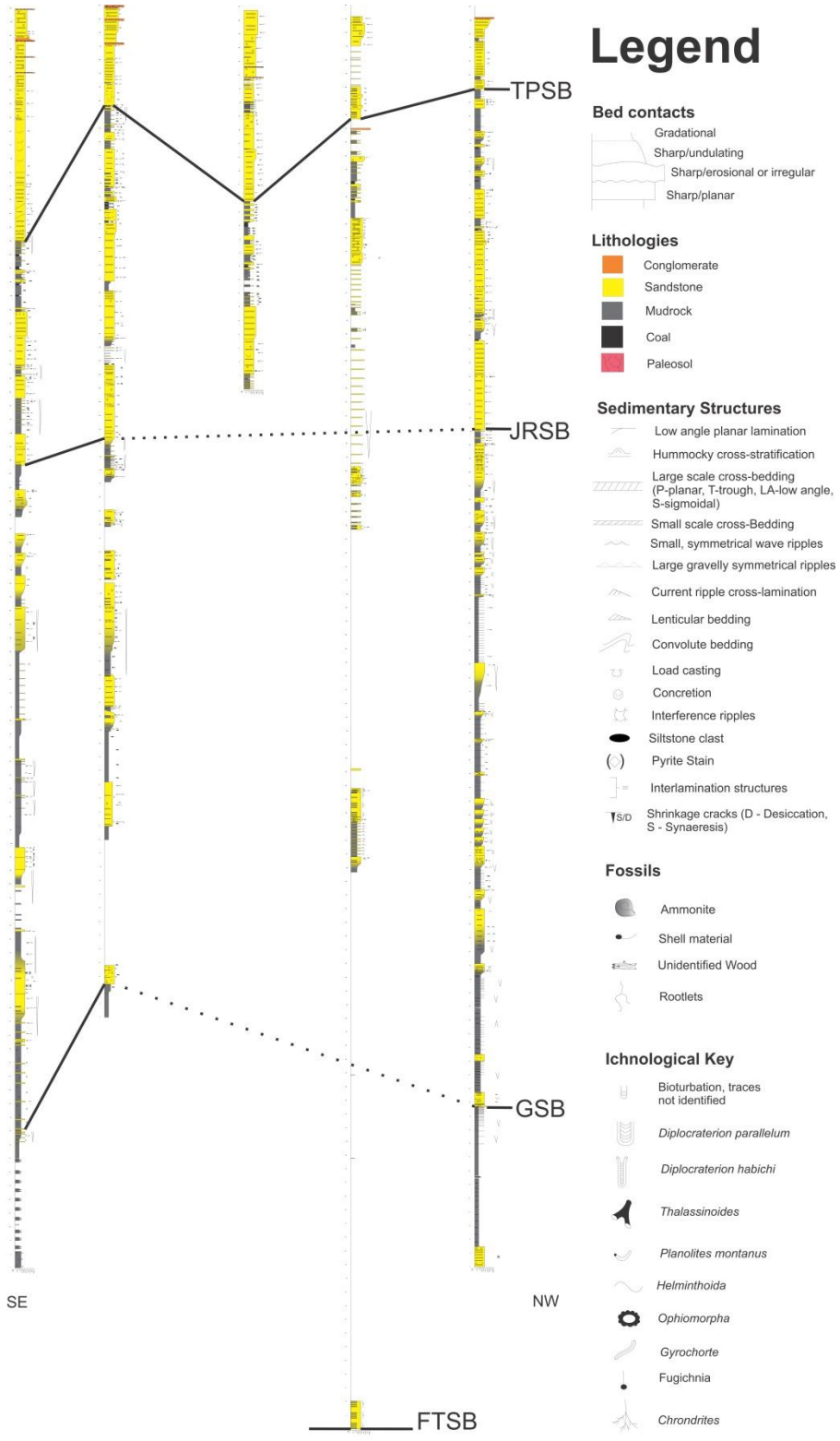

Figure 17: Stratigraphic sequences of the Mesaverde Group and the variance between the 5 logged sections, showing a thinning of sequences towards the southeast.

The Gebo Sequence is marked at its base by a major dislocation of proximal facies on top of basinal marine facies. This dislocation of facies is more pronounced in the northern measured vertical sections than those in the south (Fig. 17). In the north, the base of the sequence is represented by an incised estuarine deposit on top of prodelta deposits (Fig.18). The incised estuary deposits are overlain by proximal delta front facies and prodelta facies arranged in a fining upwards sequence. Following this fining upwards sequence are multiple coarsening upwards cycles composed of prodelta facies deposits, distal delta front facies deposits and proximal delta front facies deposits. The arrangements of these facies indicate first a deepening trend, represented by the change from incised estuary facies through to prodelta facies, followed by repeating periods of shallowing, represented by the repeated coarsening upwards cycles. This facies grouping is comparable with a transgressive systems tract represented by the deepening trend above the incised estuary facies at the base of the Gebo Sequence. The transgressive systems tract is followed by a highstand systems tract, represented by the repeated coarsening upwards cycles, and a shift towards more proximal facies deposits.

The Judith River Sequence is marked at its base by a major dislocation of facies with mouth bar facies abruptly overlying prodelta facies (Fig. 18). This dislocation is clear in localities one and four, but is not represented distinctly in any of the other localities due to poorer quality exposure (Fig. 17). The facies above the mouth bar interval are repeated alternations of mouth bar facies and coastal mire facies deposits. This indicates a proximal environment with repeated cycles of shallowing. The repeated shallowing-upward cycles combined with the proximal facies is comparable to a highstand systems tract, in which the sediment supply is greater than the rise in sea level.

Within the Judith River Sequence there are other possible sequence boundaries. There are incised bases to some of the highstand systems tract sandstone bodies that could be indicative of sequence boundaries, but none of these contacts are traceable through all of the localities and so it is not possible to define additional sequences.

The base of the Teapot Sequence is marked by an incised surface that cuts down into underlying coastal platform facies (coastal mire). Although this distributary channel incision need not represent a sequence boundary, the laterally extensive nature of this surface across the study area would suggest an external forcing control (Fig. 18). The sequence itself is composed of stacked, amalgamated distributary channel deposits with erosional incisions between bodies. Sandstone bodies become coarser-grained towards the top of the Teapot Sequence. The composition of facies within this sequence indicates no change in the formative water depth of the sequence, which stays shallow throughout. The aggradational stacking of the facies and the lack of facies change suggests that this sequence preserves stacked, lowstand systems tract deposits caused by high sediment input and sustained low base level of the system.

The increase in the degree of amalgamation of sandstone bodies in the higher sequences within the Mesaverde Group, combined with the change to more proximal facies present within the sequences, indicates a decrease in accommodation within the system over time (Fig. 18). There is a similar lateral facies change from more amalgamated proximal bodies in the northwest to more isolated distal bodies in the southeast, which is consistent with the dominant direction of sediment dispersal within the area (Fig. 17).

The stratigraphic analysis from this study is compatible with previous work both regionally across Wyoming (Fitzsimmons & Johnson 2000) and in the southern Bighorn Basin (Swift et al. 2008) (Fig. 18). There are only minor variations in the position of the sequence boundary within the Eagle Formation. Other studies such as Condon (2000) do not show any sequence boundaries between the Eagle Sandstone and underlying shale unit or between the Claggett Shale and the Judith River Formation. This poor preservation of sequence boundaries is likely due to the poorer preservation of the sandstones and sedimentary structures seen in more distal parts of the system leading to a lack of recognition of sequence boundaries. This study shows the variability of preservation of sedimentary structure from areas of proximal deposition to distal deposition within the Mesaverde Group as a major factor in the recognition of sequence boundaries (Fig. 19). This can lead to misidentification of sequence boundaries due to absences of features that would be used to identify the boundary such as a sharp based sandstone above fine grained marine deposits. The variability in the preservation of features in both proximal and distal settings could be responsible for the variations in the sequence stratigraphy and sequence boundary identification within the Mesaverde among different researchers.

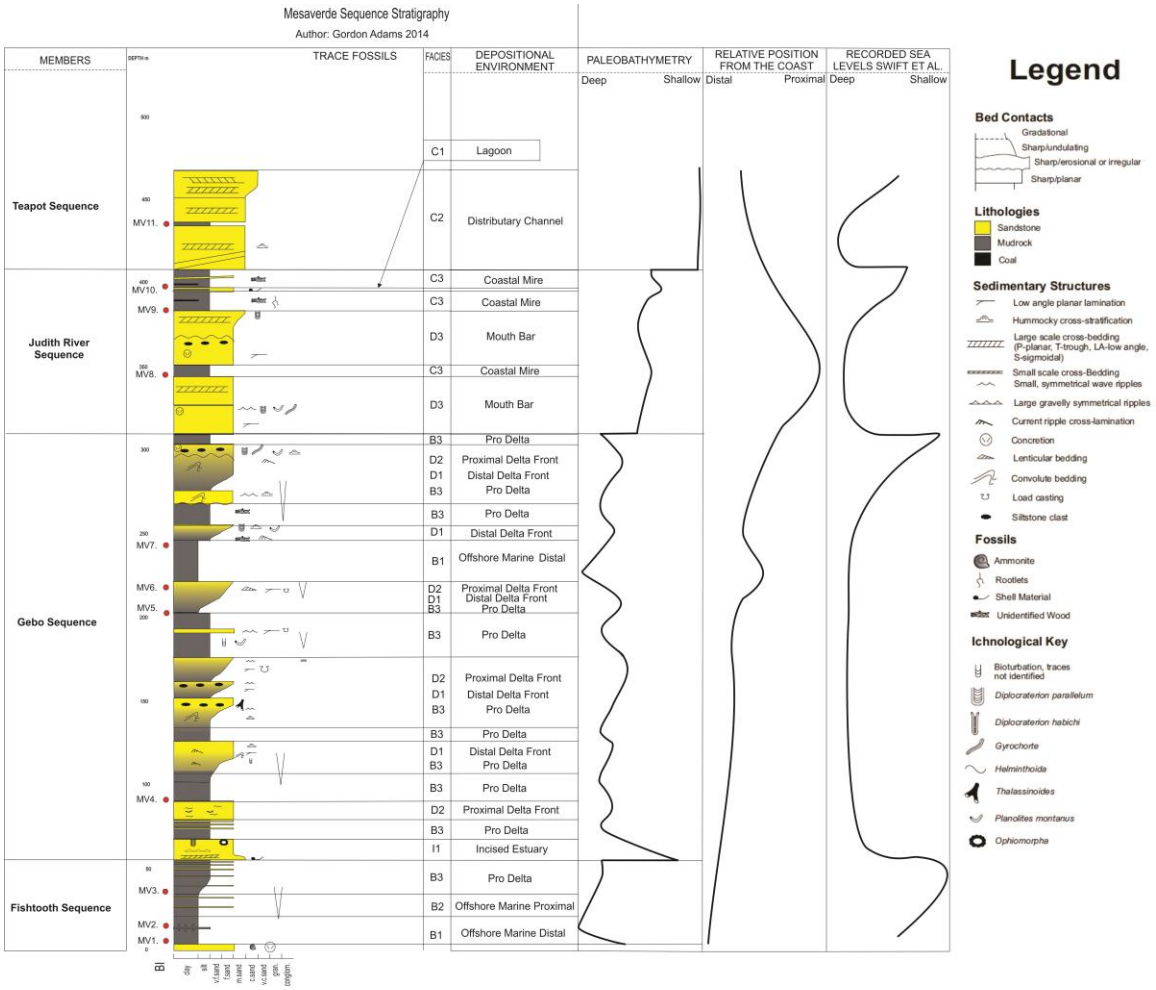

Figure 18: Paleobathymetry of the Mesaverde Group composite section showing four sequences. Also included is the relative position of deposition from factor analysis showing a proximal shift over time with the exception of the last two samples similar to the paleobathymetry. Also shown is recorded sea level from Swift et al. (2008), showing four sequences of sea level change similar to what s seen in this study.

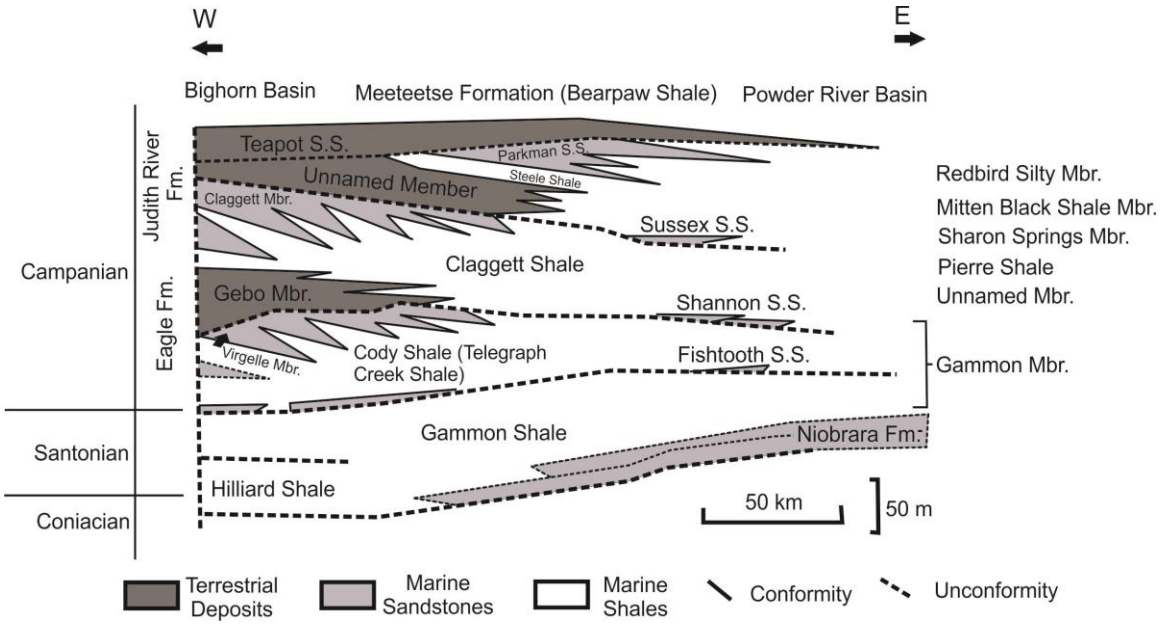

Figure 19: Coniacian – Campanian alloformations from Bighorn Basin to Wind River Basin. Fm stands for formation, SS for sandstone, and Mbr. for member. Modified from Swift et al. (2008).

Conclusions

A detailed study conducted on a 27 km transect of the Campanian Mesaverde Group of the northern Bighorn Basin coupled with a palynofacies analysis allowed for a detailed stratigraphic analysis and depositional environmental analysis of the Mesaverde Group. Facies associations present within the Mesaverde Group include basinal, delta front, coastal platform and incised estuary. The lithofacies analysis and palynofacies analysis both indicate a predominantly deltaic depositional environment throughout the Mesaverde Group. This is consistent with previous work done in southern Wyoming and in Montana. The overall direction of sediment dispersal in the section is towards the southeast, which is consistent with the dispersal from the Sevier Orogenic Belt.

The Mesaverde Group shows a progressive upward stratigraphic change from a distal to proximal environment. This change indicates a decrease in accommodation space over time through the deposition of the Mesaverde Group. The Mesaverde also

shows a change from proximal to distal depositional environment towards the southeast, which is consistent with the dominant direction of sediment dispersal within the area. This is consistent with the thinner sandstone beds seen in the Powder River Basin in southeastern Wyoming.

The stratigraphy of the Mesaverde Group indicated four depositional sequences. In this study they are identified as the Fishtooth Sequence, the Gebo Sequence, the Judith River Sequence and the Teapot Sequence. This stratigraphic sequence is consistent with that of Fitzsimmons & Johnson (2000) from the southwestern Bighorn Basin and Swift et al. (2008) regionally across Wyoming.

This study indicates a consistent sequence stratigraphy across the entire region of Wyoming due to similar lithofacies and stacking patterns. The depositional environment indicated in this study is dominantly deltaic, and while it is consistent with some previous studies, is not fully consistent with others. However, with the change in sedimentary structure, abundance and preservation towards the southeast of this section, the lithofacies from other studies could show less deltaic features than seen in this study. The addition of the palynofacies data allows for a clearer interpretation even with poor preservation of sedimentary structures.

Bibliography

Bann, K.L., Fielding, C.R., MacEachern, J.A., and Tye, S.C. (2008) Ichnological and sedimentologic signatures of mixed wave-and storm-dominated deltaic deposits: Permian Pebbley Beach Formation, Sydney Basin, Australia; *in* McIlroy, D., ed., The application of ichnology to paleoenvironmental and stratigraphic analysis: Geological Society of London Special Publication, 228: 179 – 211.

Batten, D.J. (1996) Chapter 26A. Palynofacies and paleoenvironmental interpretation; *in* Jansonius, J. &McGregor, D. C. (ed.), Palynology: principles and applications; American Association of Stratigraphic Palynologists Foundation, v. 3, p. 1011-1064.

Catuneanu, O. (2006) Principles of sequence stratigraphy: Elsevier: 375 pp.

Clark, C.K. (2010) Stratigraphy, sedimentology, and ichonology of the Upper Cretaceous Frontier Formation in the Alkali Anticline region, Bighorn County, Wyoming: Masters Thesis, University of Nebraska-Lincoln: p. 57.

Condon, S.M (2000) Stratigraphic Framework of Lower and Upper Cretaceous Rocks in Central and Eastern Montana: U.S. Geological Survey Digital Data Series DDS-57.

Crews, G. C., Barlow Jr., J. A., Haun, J. D. (1976) Upper Cretaceous Gammon, Shannon, and Sussex Sandstones, Central Powder River Basin, Wyoming: Wyoming Geological Association Guidebook, 28th Annual Field Conference, p.9-20.

Dennison, J. M., and Hay, W. W. (1967) Estimating the needed sampling area for subaquatic ecologic studies: Journal of Paleontology, v. 41, no. 3, pp. 706-708.

Fitzsimmons, R.J., and Johnson, S.D. (2000) Forced regressions: recognition, architecture and genesis in the Campanian of the Bighorn Basin, Wyoming, in Hunt, D., and Gawthorpe. R.L., eds., Sedimentary Responses to Forced Regressions: Geological Society of London, Special Publication 172, p. 113-139.

Gill, J.R., and Cobban, W.A. (1966) The Red Bird section of the Upper Cretaceous Pierre Shale in Wyoming: U.S. Geological Survey Professional Paper 393-A, 73.

Gill, J.R., and Cobban, W A. (1973) Stratigraphy and geologic history of the Montana Group and equivalent rocks, Montana, Wyoming, and North and South Dakota. U.S. Geological Survey Professional Paper 776, p. 1-35.

Hammer, Ø. (2014) PAST PAleontological STatistics Version 3.04 Reference Manual: Natural History Museum, University of Oslo, pdf accessed online 1/31/15, http://folk.uio.no/ohammer/past/index.html

Hammer, Ø. and Harper, D. (2006) Paleontological Data Analysis: Blackwell Publishing.

Jacka, A.D., (1965) Depositional dynamics of the Almond Formation, Rock Springs Uplift, Wyoming: Wyoming Geological Association, 19th Field Conference Guidebook, p. 81-100.

Johnson, R. C., Keefer, W. R., Keighin, C. W. and Finn, T.M. (1998) Detailed Outcrop Studies of the Upper Part of the Upper Cretaceous Cody Shale and the Upper

Cretaceous Mesaverde, Meeteetse, and Lance Formations, Bighorn Basin, Wyoming: Cretaceous and Lower Tertiary Rocks of the Bighorn Basin, Wyoming and Montana; 49th Annual Field Conference Guidebook, p. 59-78.

Keefer, W.R., Finn, T.M., and Keighin, C.W. (1998) Regional stratigraphy and correlation of Cretaceous and Paleocene rocks, Bighorn Basin, Wyoming and Montana: Wyoming Geological Survey. 49th annual field conference guidebook, p. 1-35.

Kieft, R.L., Hampson, G.J., Jackson, C.A.L., Larsen, E. (2011) Stratigraphic Architecture of a Net-Transgressive Marginal – to Shallow Marine Succession: Upper Almond Formation, Rock Springs Uplift, Wyoming, U.S.A.: Journal of Sedimentary Research, v. 81, p. 513-533.

Klovan, J. E., and Imbrie, J. (1971) An Algorithm and FORTRAN-IV Program for Large-Scale *Q*-Mode Factor Analysis and Calculation of Factor Scores: Mathematical Geology, v. 3, no. 1, p. 61-77.

Klug, B. (1994) The Mesaverde Group (Campanian) in the Bighorn Basin of Wyoming / Montana, USA: Bonner Geowissenschaftliche Schriften, v. 16 (University of Bonn, Germany, doctoral dissertation), p.199.

Lawlor, R.E. (1956) Cretaceous Stratigraphy of Central Montana: Montana Geological Society 2010, Billings Geological Society, Guidebook: 7th Annual Field Conference, p. 31-34.

Martinsen, O. J., Martinsen, R.S., and Steidtmann, J. R. (1995) Mesaverde Group (Upper Cretaceous), Southeastern Wyoming: Allostratigraphy Versus Sequence Stratigraphy in a Tectonically active Area: American Association of Petroleum Geologists Bulletin v. 77, no. 8, (Aug. 1993) p. 1351-1373.

McGookey, D.P., Haun, J.P.,Heele, L.A., Goodell, H.G., McCubbin, D.G., Wiemer, R.J., and Wulf, G.R. (1972) Cretaceous system *in* Mallory, W.W., ed., Geologic Map of the Rocky Mountain Region: Rocky Mountain Association of Geologists, p. 190-233.

Mellere, D, and Steele, R. (1995) Variability of Lowstand Wedges and their Direction from Forced-Regressive Wedges in the Mesaverde Group, Southeast Wyoming: Geology, v. 23, p. 803-806.

Oboh-Ikuenobe, F.E., Obi, C.G., and Jaramillo, C.A. (2005) Lithofacies, palynofacies, and sequence stratigraphy of Palaeogene strata in Southeastern Nigeria: Journal of African Earth Science. v. 41, p. 79-102.

Purcell, T.E. (1960) The Mesaverde Formation of the North and Central Powder River Basin, Wyoming: The Shale Shaker Digest III. v. IX – XI, p. 357-374.

Reiss, E.J. (2013) Stratigraphy and Paleo-environment of the Campanian Mesaverde Formation, Big Horn Basin, Wyoming: University of Nebraska Lincoln, McNair Scholars Program, unpublished.

Rice, D.D. (1980) Coastal and deltaic sedimentation of Upper Cretaceous Eagle Sandstone: relation to shallow gas accumulations, north-central Montana: AAPG Bulletin, v. 64, p. 316-338.

Rich, E.I. (1958) Stratigraphic relation of latest Cretaceous rocks in parts of Powder River, Wind River and Big Horn Basins, Wyoming: Bulletin of AAPG. v. 42 no. 10, p. 2424-2443.

Roehler, H.W. (1990) Stratigraphy of the Mesaverde Groups in the Central and Eastern Greater Green River Basin, Wyoming, Colorado, and Utah: U.S. Geological Survey Professional Paper 1508.

Severn, W.P. (1961) General Stratigraphy of the Mesaverde Group, Bighorn Basin, Wyoming: Wyoming Geological Association Symposium on Late Cretaceous Rocks, Wyoming and Adjacent Areas, 16th annual Field Conference Guide Book, p.195-199.

Summerhayes, C.P. (1987) Organic-rich Cretaceous sediments from the North Atlantic. In: Brooks, J. and Fleet, A.J., (eds) Marine Petroleum Source Rocks. Geological Society Special Publication, 26, p. 301-316.

Swift, D. J. P., Parson, S. B., Howell, K. A. (2008) Campanian Continental and hallow marine architecture in a eustatically modified clastic wedge: Mesa Verde Group, Wyoming, U.S.A.: Recent Advances in Models of Siliciclastic Shallow-Marine Stratigraphy, SEPM Special Publication no. 90, p. 473-490.

Tschudy, B. D. (1973) Palynology of the Upper Campanian (Cretaceous) Judith River Formations, North-Central Montana: Geological Survey Professional Paper 770, U.S Department of the Interior.

Tyson, R.V. (1993) Sedimentary Organic Matter: Organic Facies and Palynofacies Analysis. Chapman and Hall, London.

Wright, L. D. (1977) Sediment transport and deposition at river mouths: A synthesis. Geological Society of America Bulletin, June, 1977, v. 88, no. 6, p. 857-86

Basinal Facies Association					
Facies	**Lithology**	**Thickness**	**Physical Structures**	**Biogenic Structures**	**Depositional Environment**
B1	Highly fissile shale. Some non-continuous siltstone beds, thin sandstone partings, bentonite beds in siltstone.	Up to 34m	Flat lamination present. No other sedimentary features.	No bioturbation present and no fossils present	Distal offshore marine
B2	Shale interbedded with siltstone. Laterally discontinuous, sandstone. Siltstone more abundant upwards (coarsening and thickening upwards).	Up to 45m	No sedimentary features present	Bored ammonite fragments. BI = 0-1. Siltstone contains comminuted plant debris.	Proximal offshore marine
B3	Siltstone with thinly interlaminated and interbedded sandstone, minor shale, carbonate concretions.	Up to 45m	Some sandstone beds show low-angle cross-stratification, ripple cross-lamination.	Rare, sporadic bioturbation (*Planolites)*.BI = 0-1.	Prodelta

Appendix 1: Facies descriptions for basinal facies associations.

Delta Front Facies Association					
Facies	**Lithology**	**Thickness**	**Physical Structures**	**Biogenic Structures**	**Depositional Environment**
D1	Thinly interbedded fine grained sandstone and siltstone.	Up to 15m	Ripple cross lamination, Interference ripples, symmetrical wave ripples and local hummocky cross-stratification.	Sporadically distributed bioturbation, comprising. *fugichnia*, *Gyrochorte*, *Diplocraterion*, *Ophiomorpha* and *Planolites*. BI = 1-3.	Distal delta front
D2	Thickly interbedded fine-grained sandstone and siltstone, arranged into crudely coarsening-upward sequences.	Up to 25m	deformed bed bases with gutter casts and large load masses. Flat and low-angle stratification, hummocky cross-stratification, less common ripple cross-lamination.	Sporadically distributed, indeterminate bioturbation, local plant debris.	Proximal delta front
D3	Thickly bedded, sharply-based fine grained sandstone, coarsening upward to medium-grained sandstone.	Up to 29m	Flat and low angle stratification, trough cross-bedding with mud drapes (locally bimodal).	Bioturbation sporadic, local comminuted plant debris.	Mouth bar

Appendix 2: Facies description for delta front facies associations.

Coastal Platform Facies Association					
Facies	**Lithology**	**Thickness**	**Physical Structures**	**Biogenic Structures**	**Depositional Environment**
C1	Thinly bedded, fine grained sandstone, interlaminated fine grained sandstone and siltstone, arranged in coarsening- and fining-upward sequences.	Up to 4m	Symmetrical wave ripples, ripple cross-lamination.	Sporadically distributed bioturbation (*Diplocraterion)*, BI =0-1. Plant rootlets and detrital plant debris, bivalve shell debris.	Lagoon
C2	Medium to coarse grained sandstone, local siltstone clasts and siltstone partings.	Up to 90m	Macroform inclined bedding, erosion surfaces, trough cross-bedding, locally bimodal and with mud drapes on foresets, flat and low-angle cross-stratification.	Sporadically distributed bioturbation (*Planolites)*, BI = 0-1 Local comminuted plant debris. Some highly broken up shell debris.	Coastal distributary channel
C3	Carbonaceous shale interbedded with thin siltstone, sandstone, and locally coal beds.	Up to 13m	Compositional layering.	Abundant plant debris ranging from comminuted to 1-2cm, in situ rootlets.	Coastal mire

Appendix 3: Facies descriptions for coastal platform facies associations.

Incised Estuary Facies Association					
Facies	**Lithology**	**Thickness**	**Physical Structures**	**Biogenic Structures**	**Depositional Environment**
I1	Fine- to medium-grained sandstone	Up to 8m	Sharp erosional base. Ripple cross lamination, interference ripples, symmetrical wave ripples and local hummocky cross-stratification, small-scale trough cross-bedding.	Sporadically distributed bioturbation, comprising: fugichnia, *Gyrochorte*, *Diplocraterion*, *Ophiomorpha* and *Planolites*. BI = 1-3. Shell fragments in some sandstone beds. Sporadic plant debris.	Incised estuary

Appendix 4: Facies description for incised estuary facies associations.

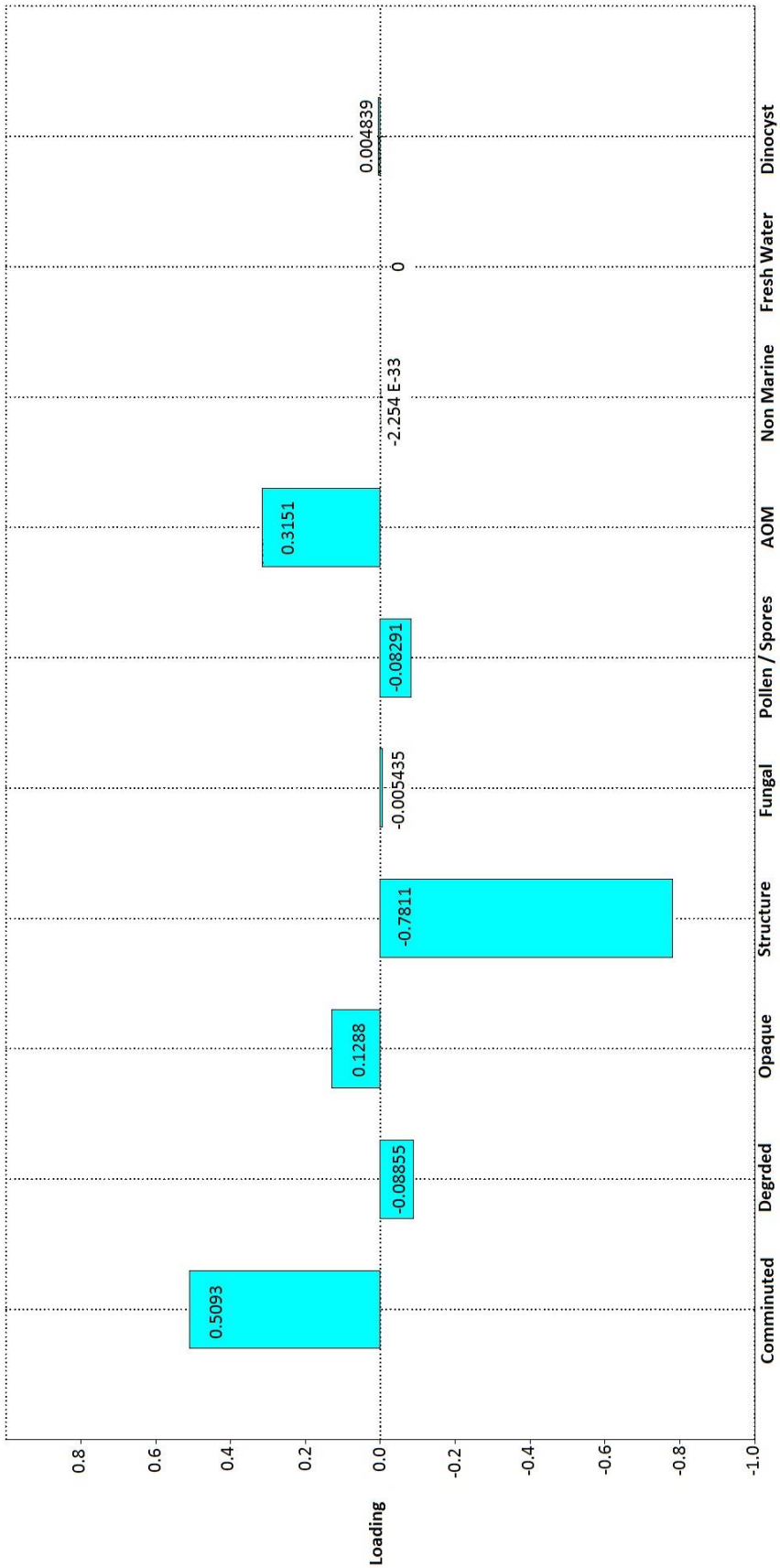

Appendix 5: Factor loading for Principal Component 1.

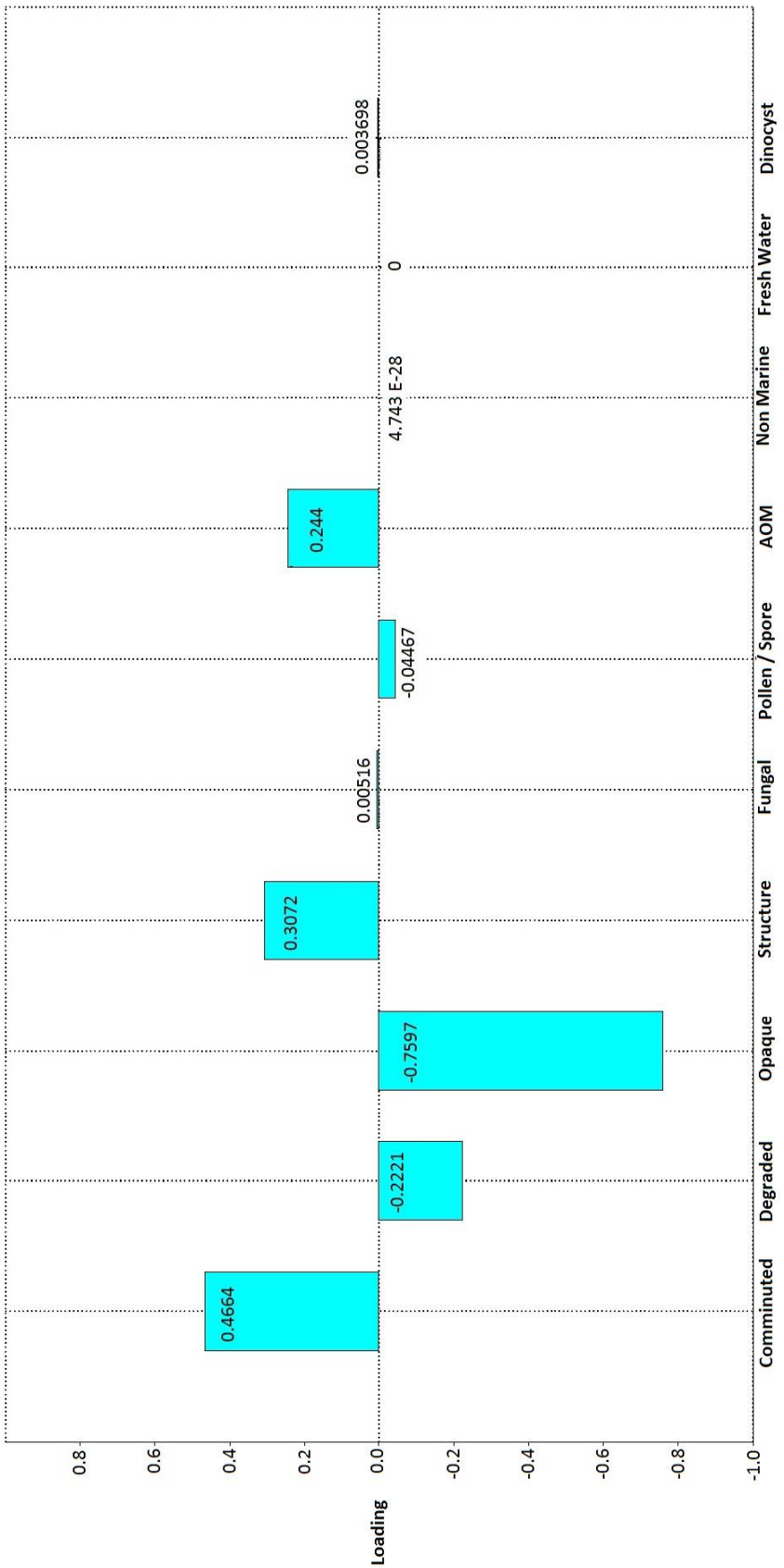

Appendix 6: Factor loading for Principal Component 2.

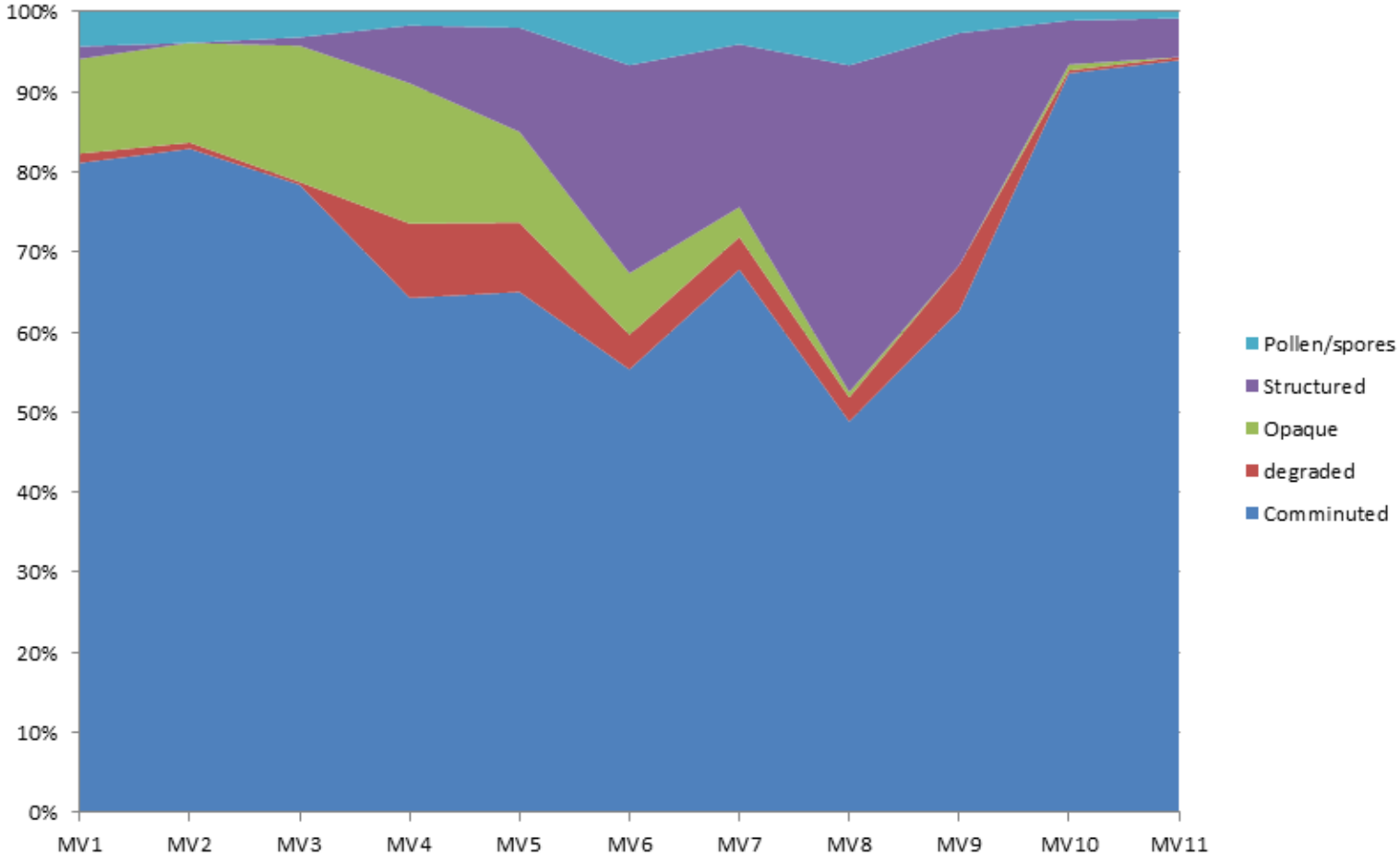

Appendix7: Diagram showing the change in terrestrial origin material over time in the Mesaverde Group. The opaques volume in decreases incrementally with time throughout the section.

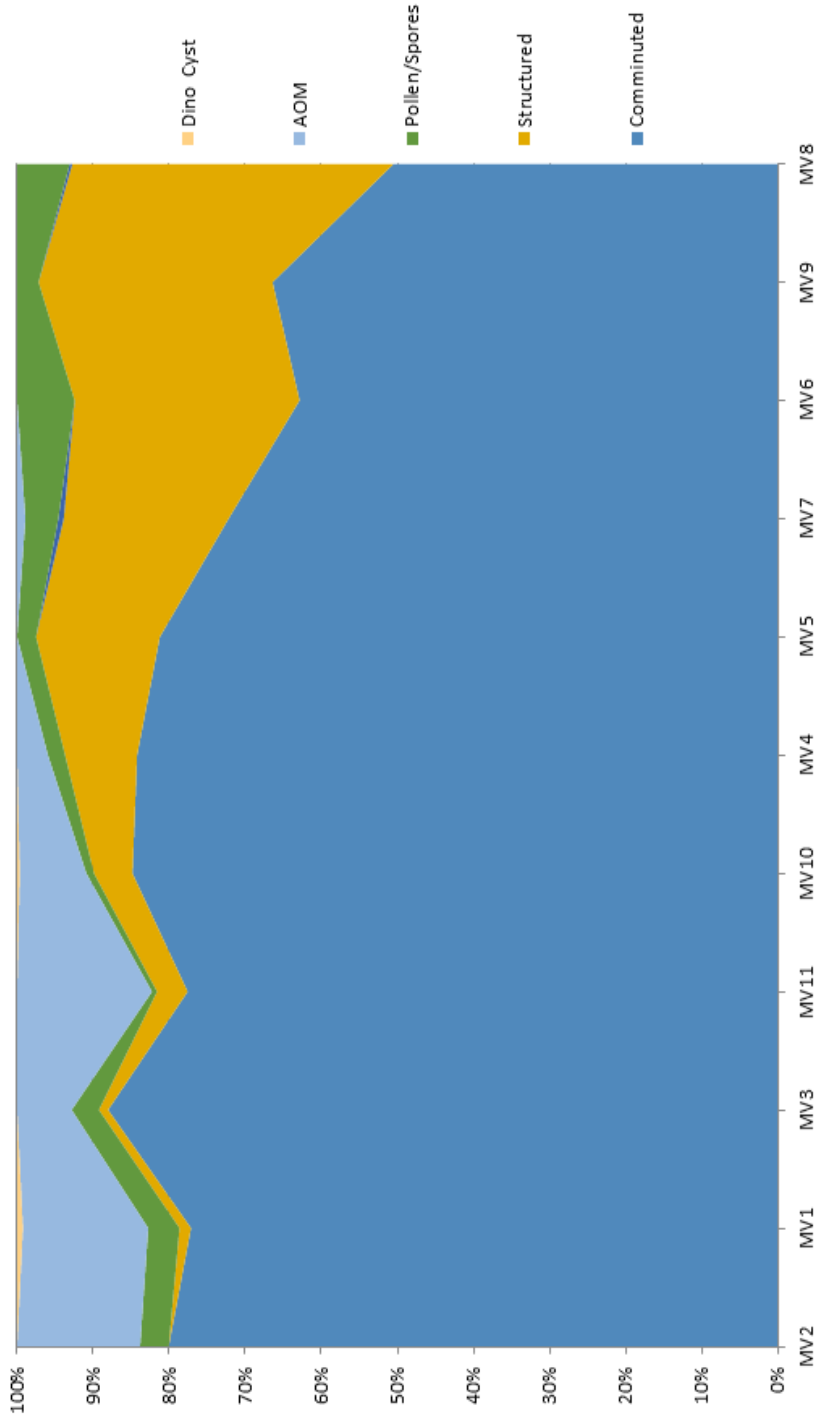

Appendix 8: Graph of major palynomoprhs arranged in order of factor analysis. Derived gradient showing a decrease in distal indicators and an increase in proximal indicators throughout the sequence.

Appendix 9: Logs of measured vertical section of this study. Position of each measured section is shown in figure 4 and facies are fully described in facies associations section.

Locality 1: Alkali Anticline 0-150m

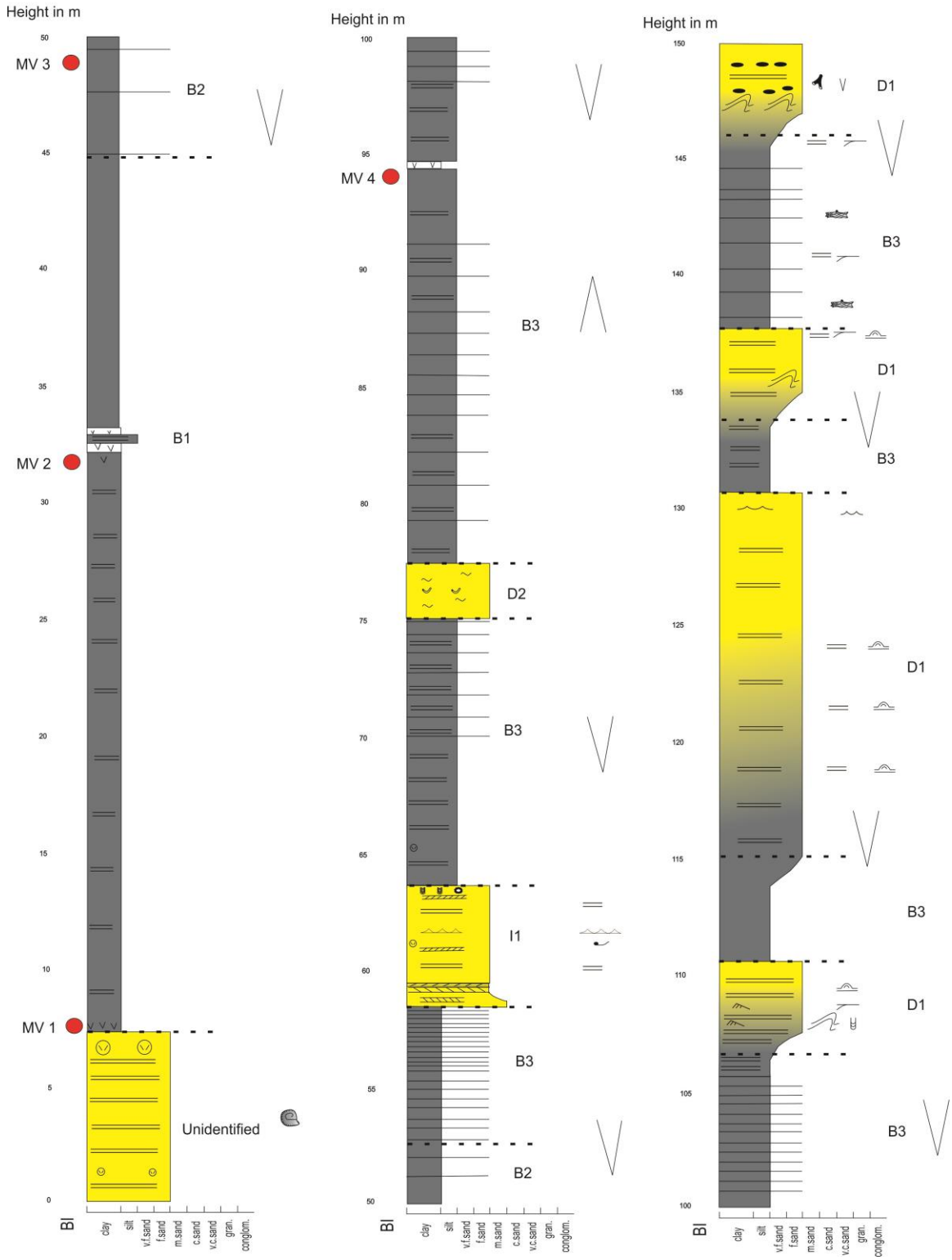

Locality 1: Alkali Anticline 150-300m

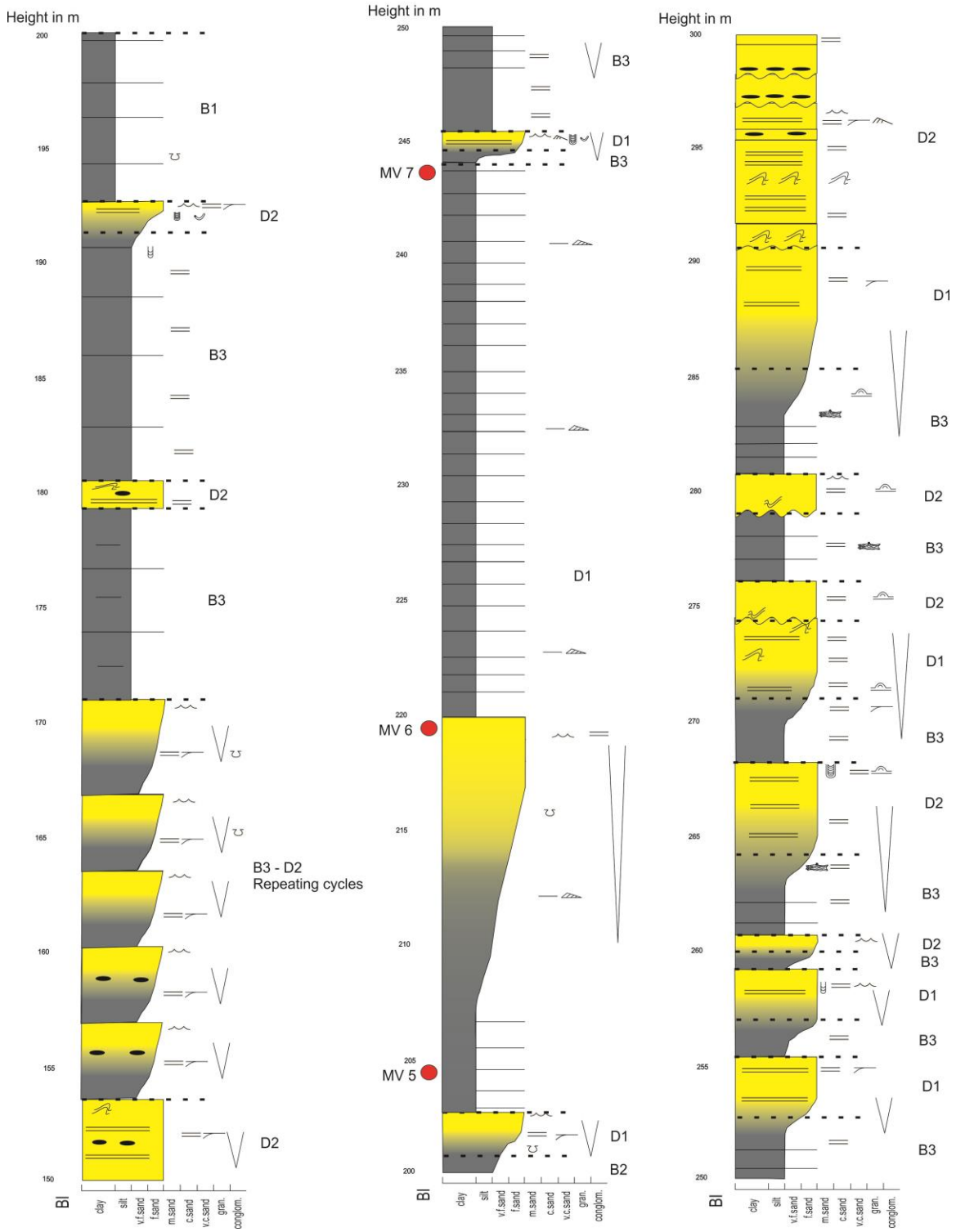

Locality 1: Alkali Anticline 301-450m

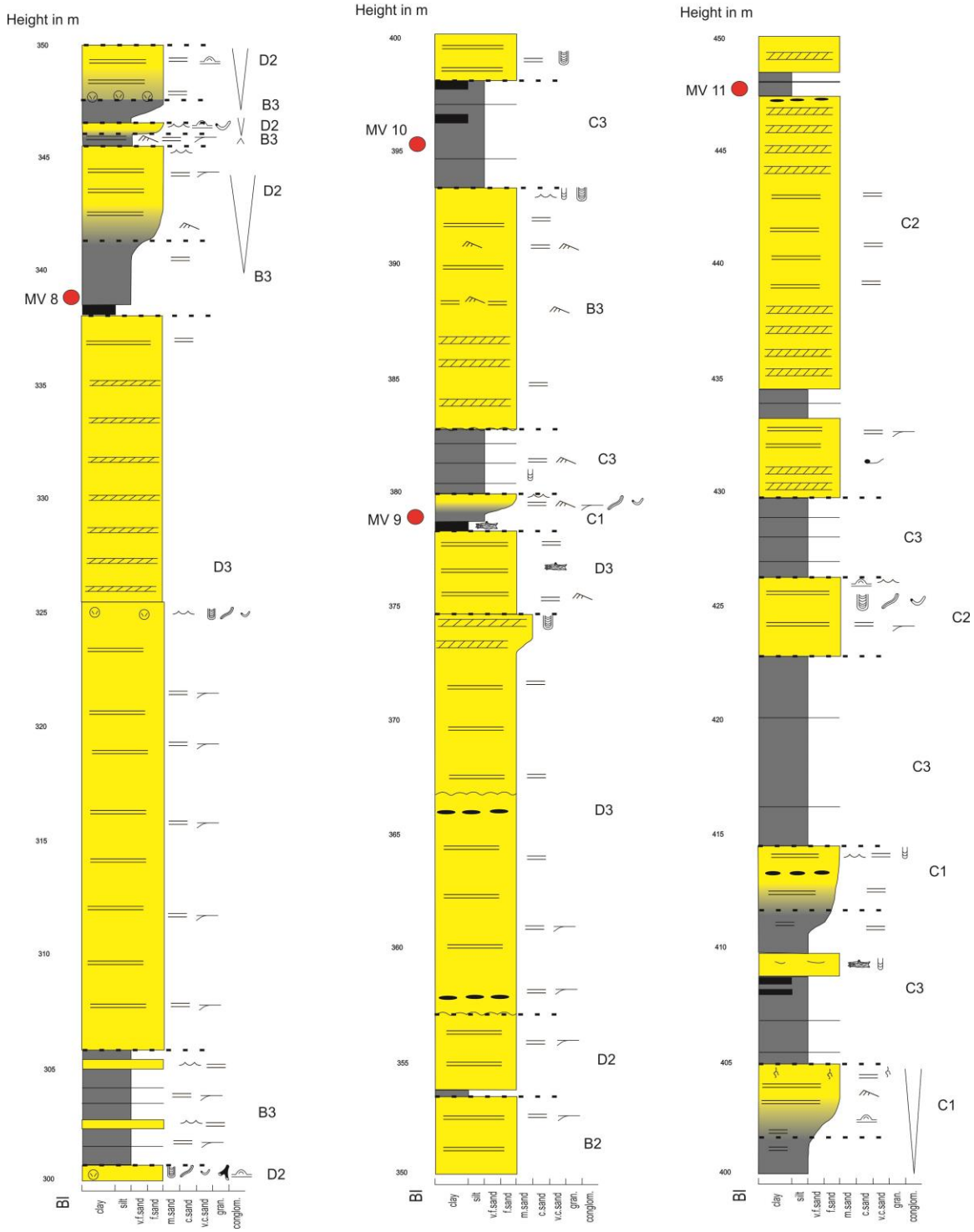

Locality 1: Alkali Anticline 451- 456 m

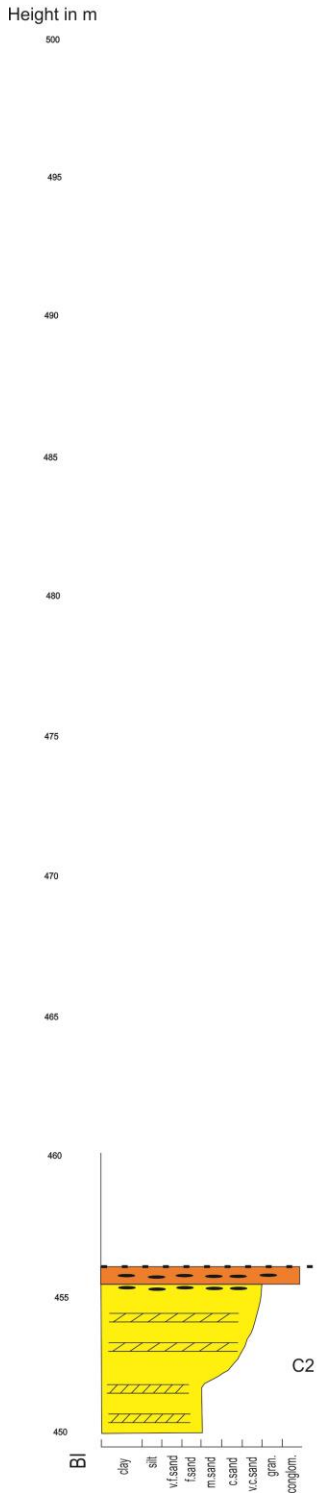

Locality 2: Large Field 0 - 425 m

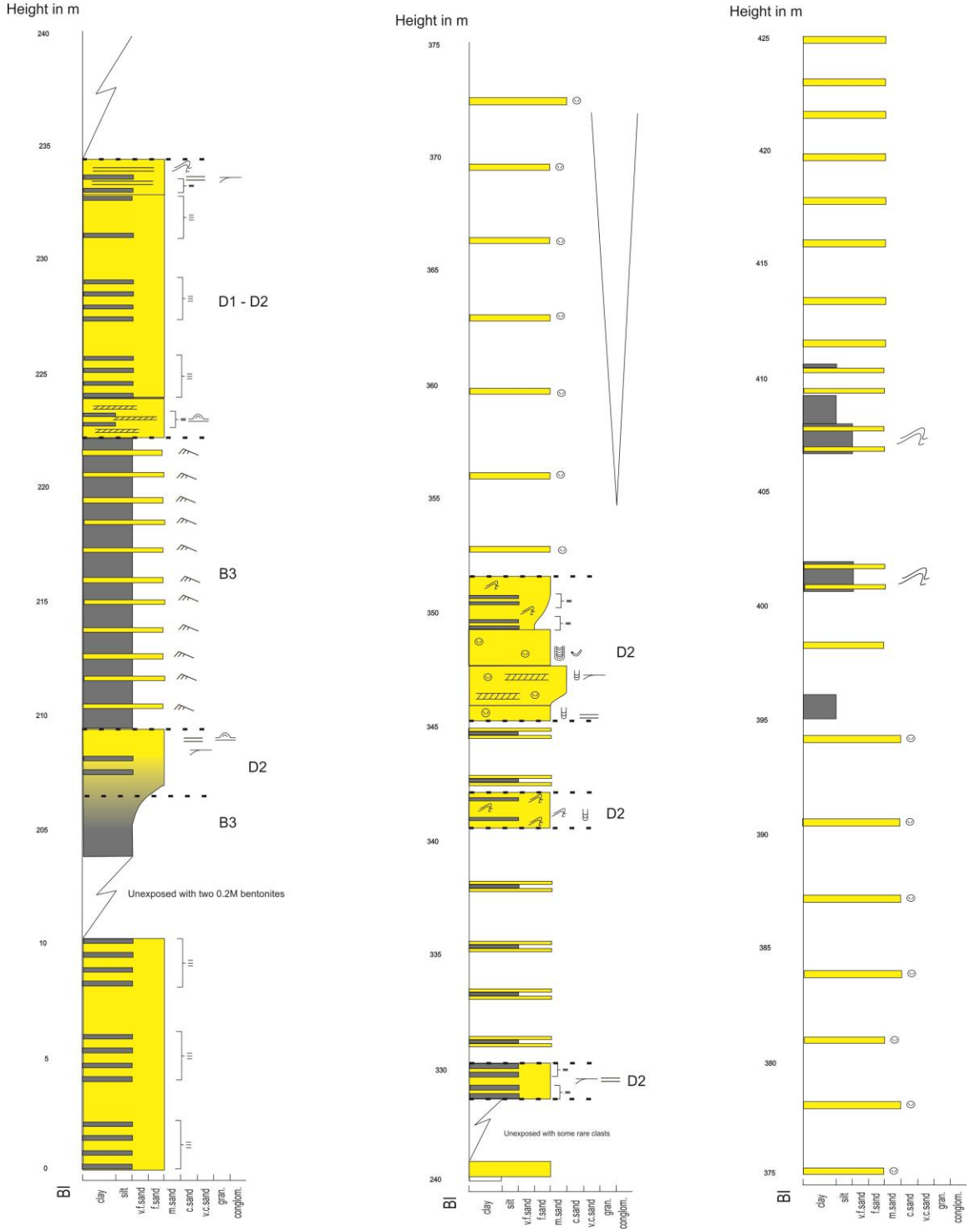

Locality 2: Large Field 425 - top m

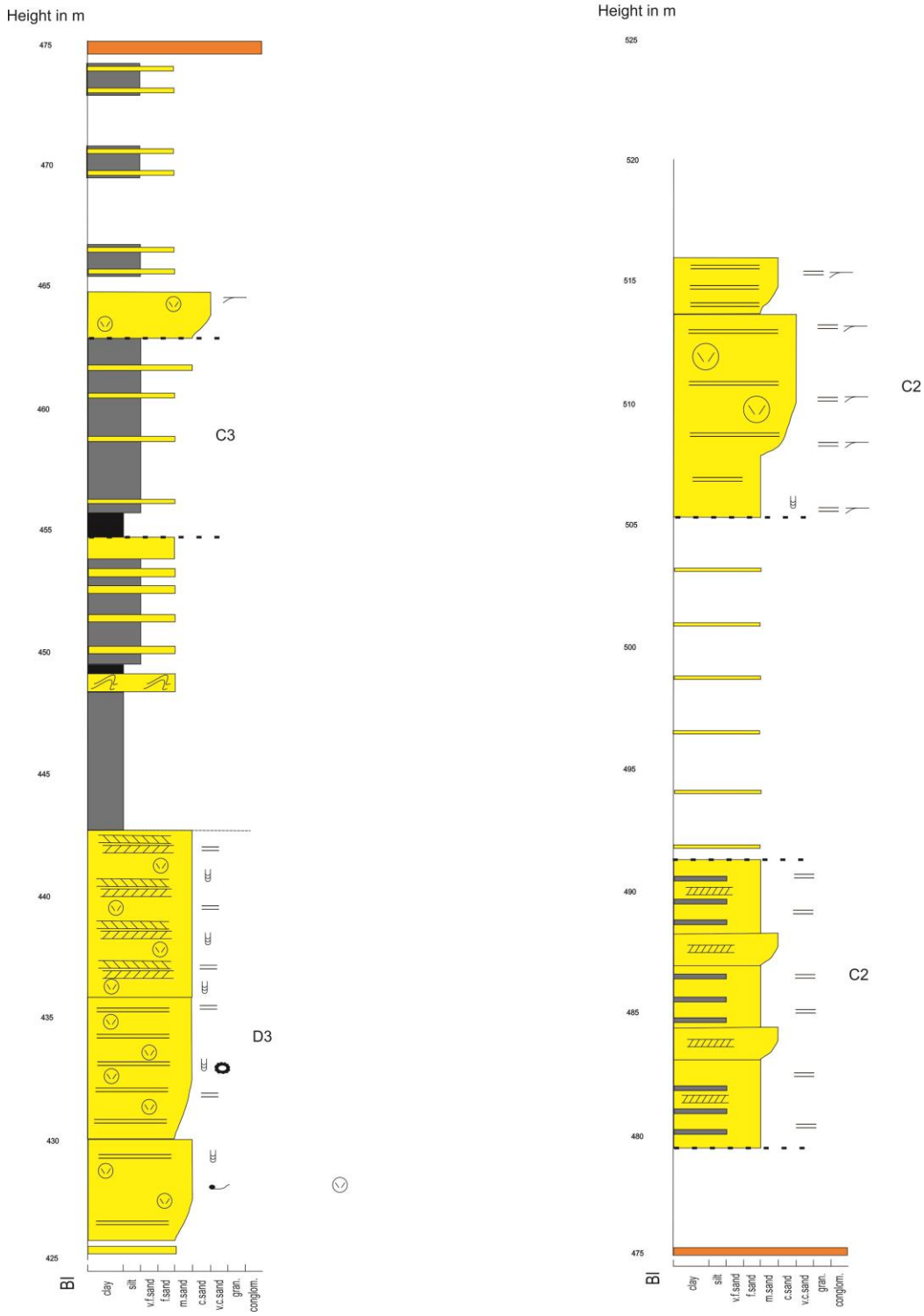

Locality 3: Greybull Bench 0 -150 m

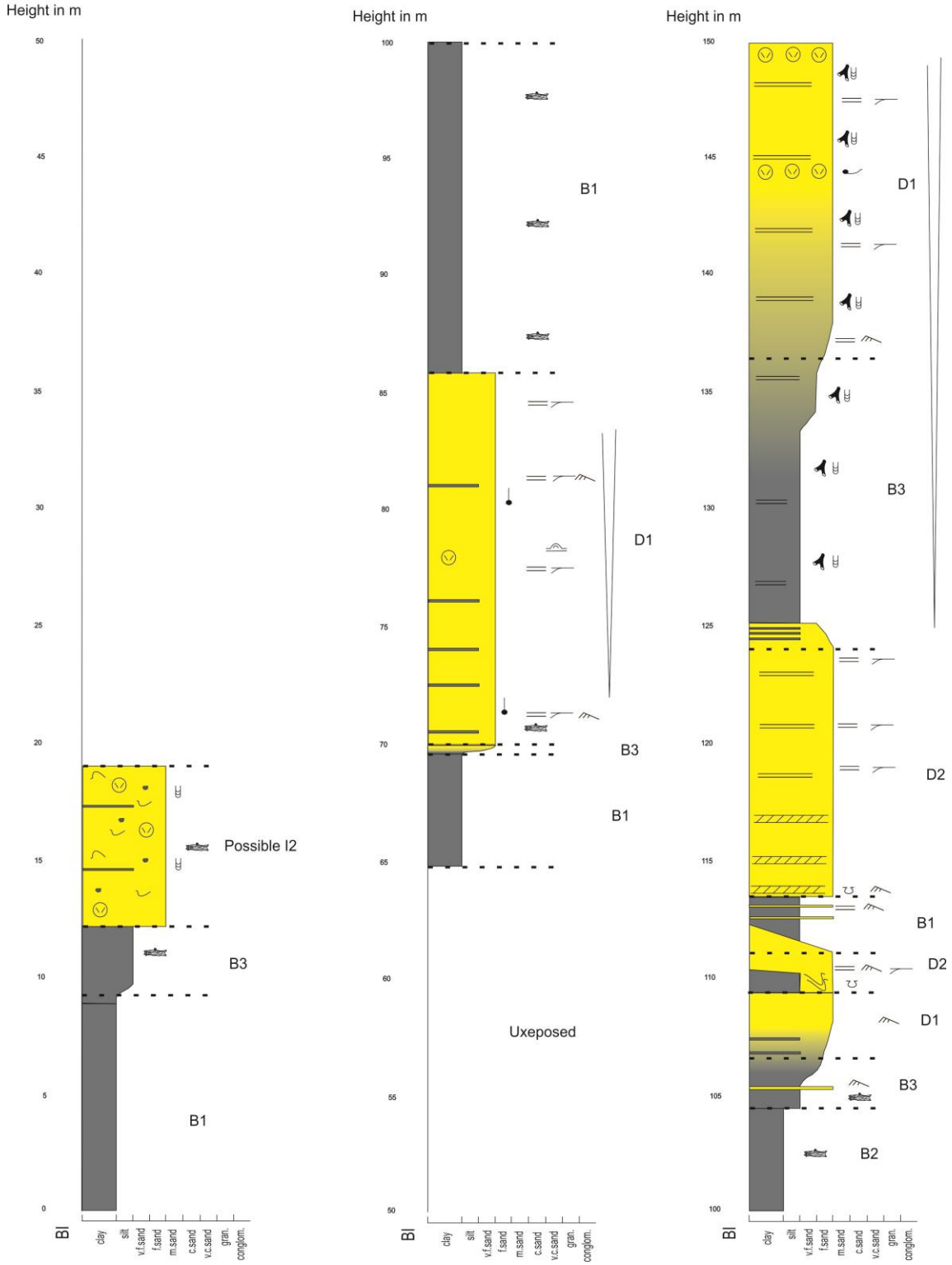

Locality 3: Greybull Bench 150 -300 m

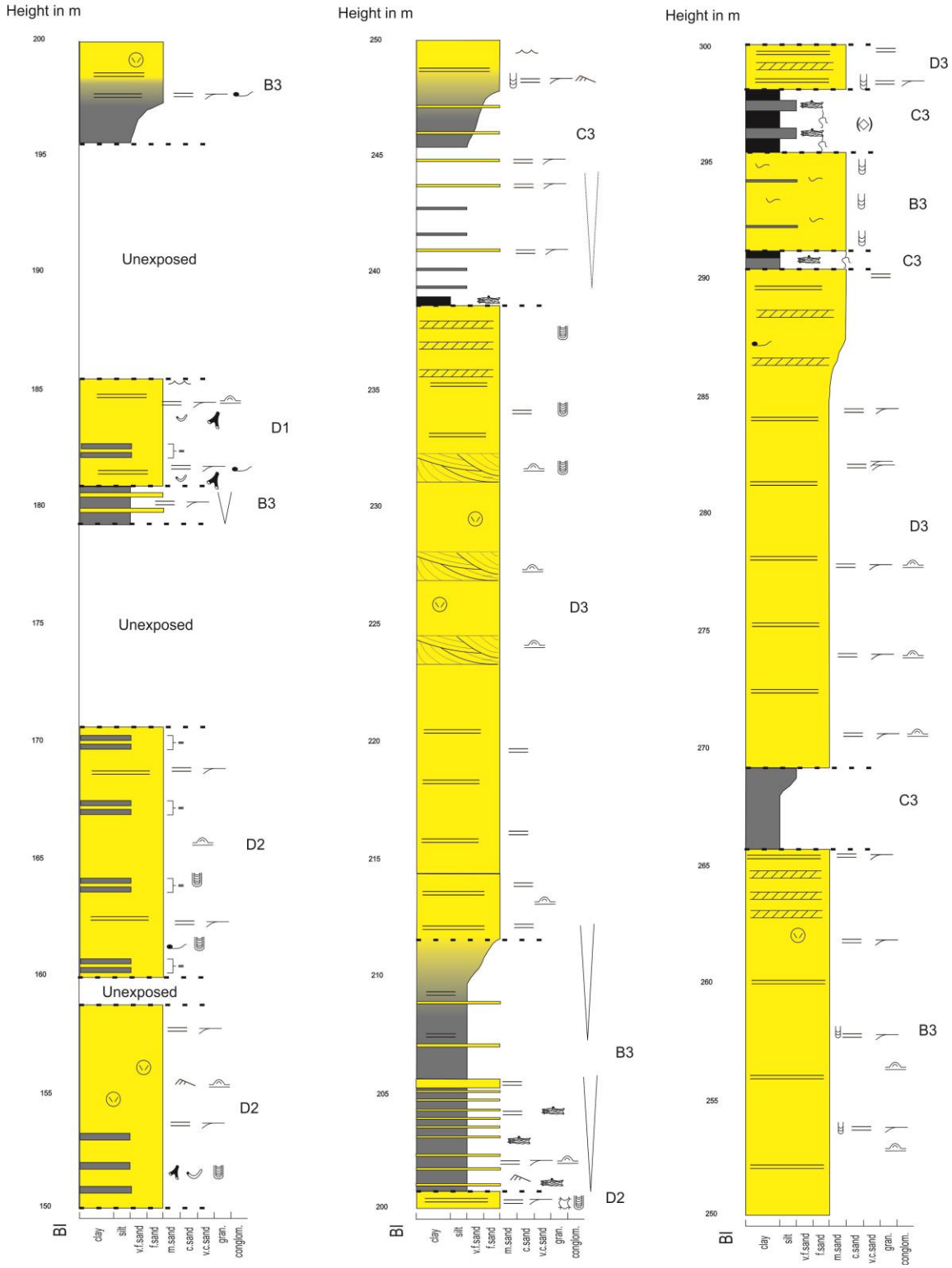

Locality 3: Greybull Bench 300 - top m

Locality 4: Little Dry Creek

Locality 5: The Casey's 0 - 150 m

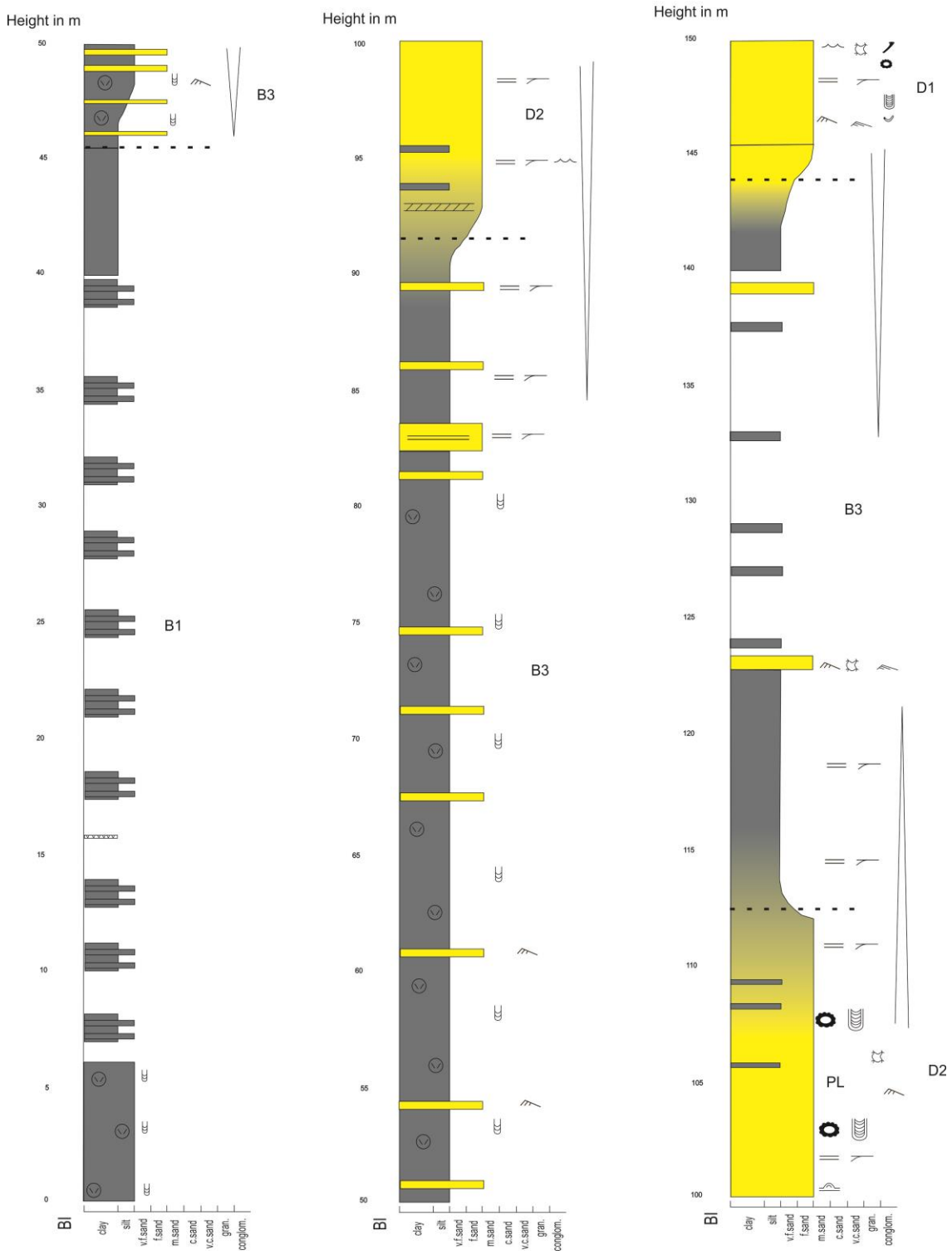

Locality 5: The Casey's 150 - 300 m

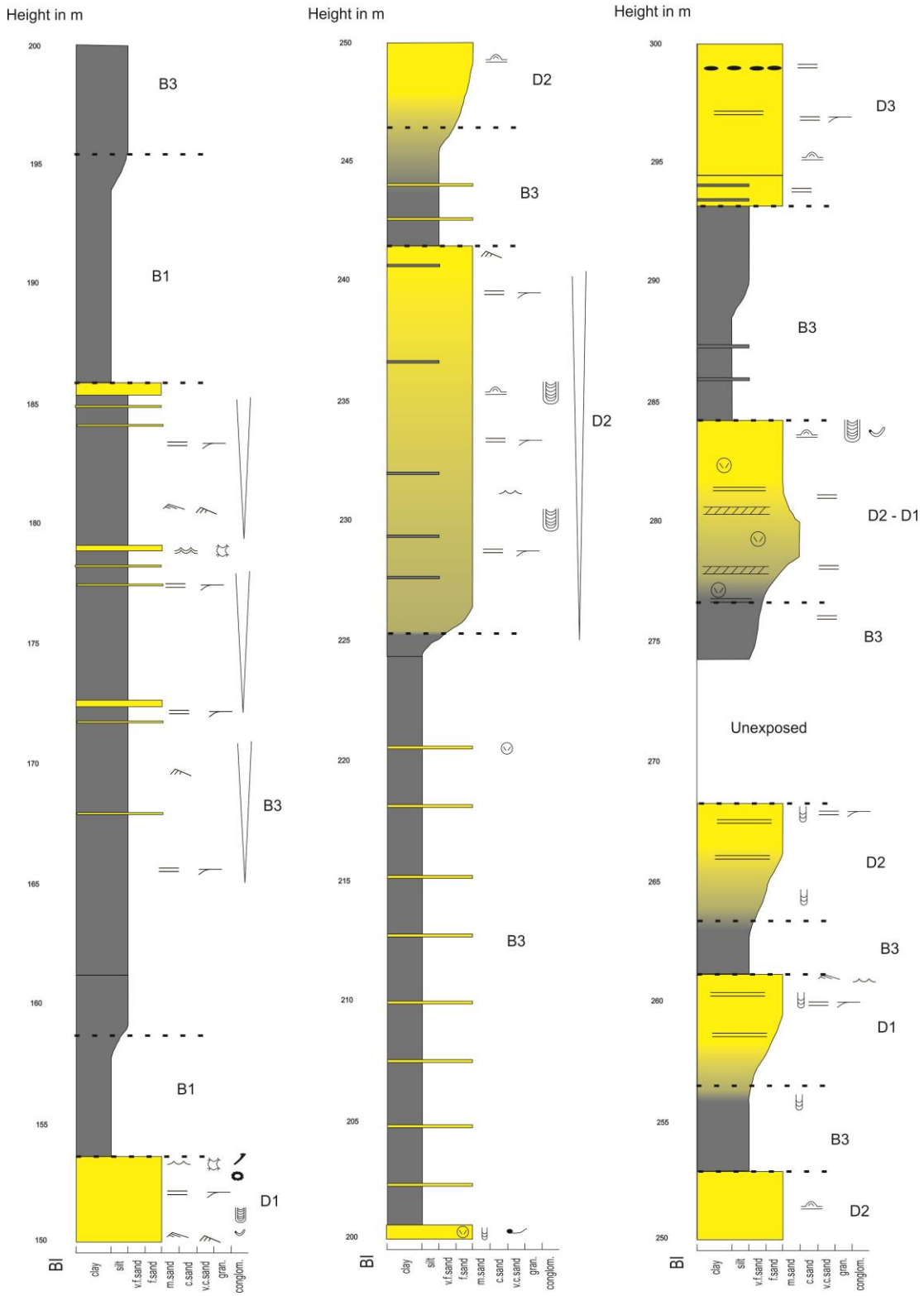

Locality 5: The Casey's 300 - 450 m

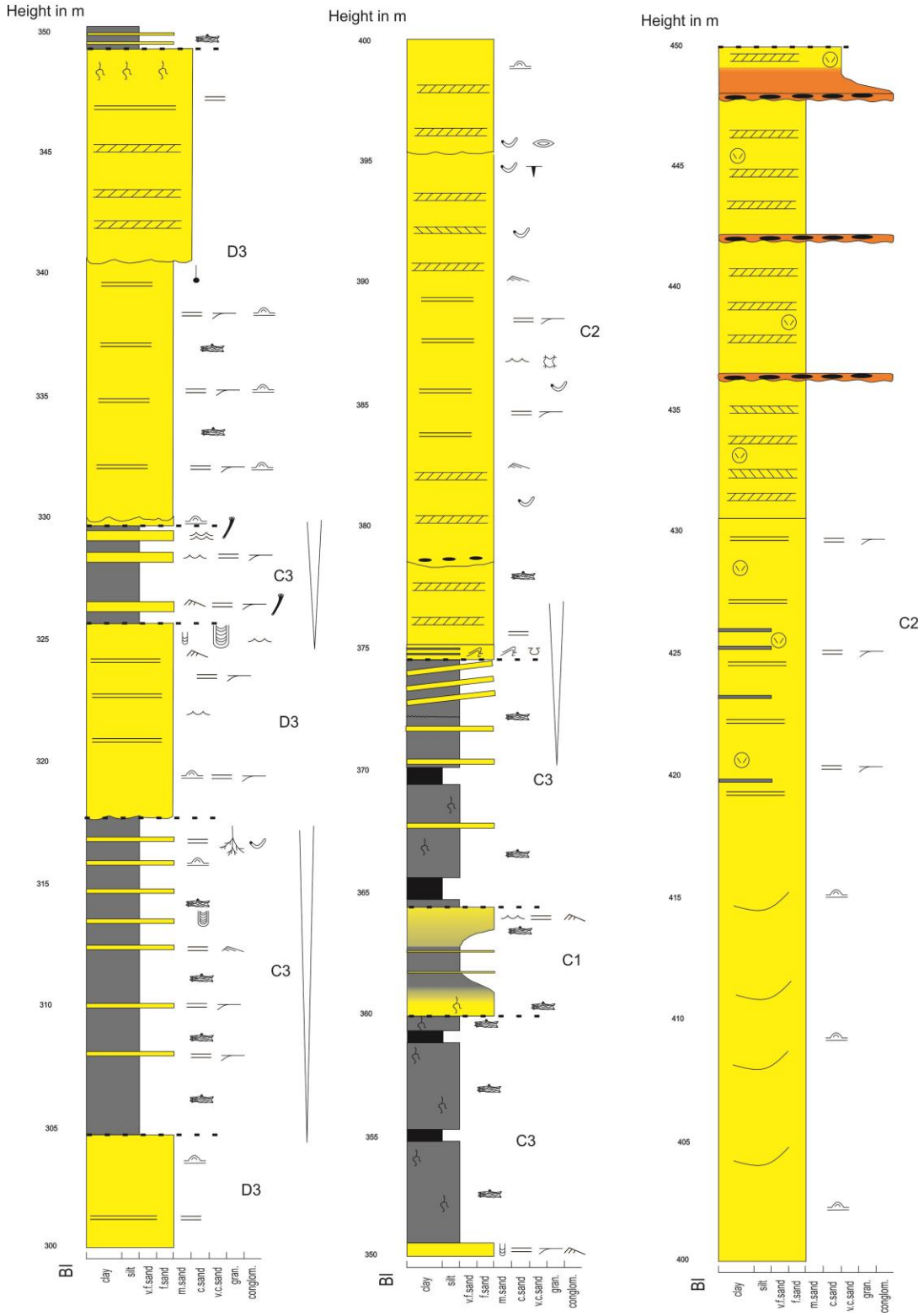

Locality 5: The Casey's 450 - top m

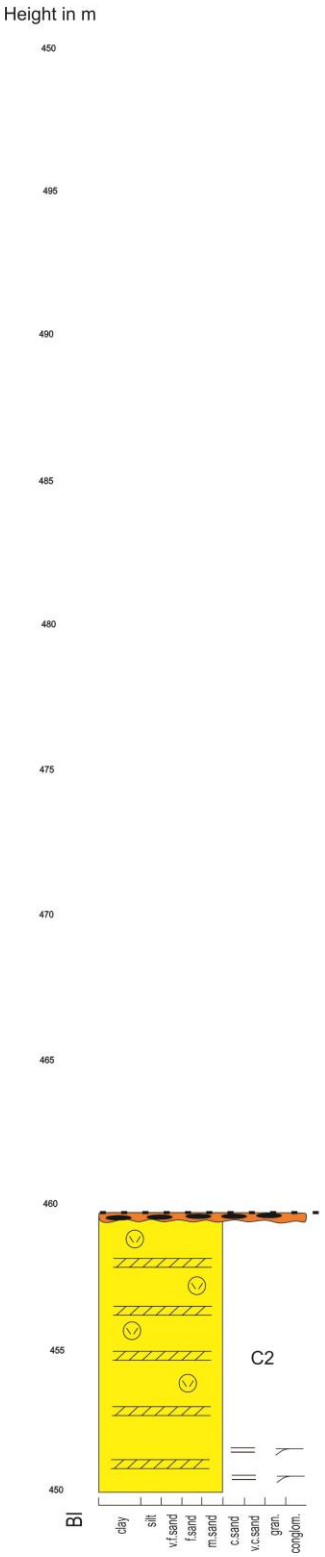

Appendix 10: Paleoflow measurements taken throughout the study. Shows which measured section and the height they were taken from. Statistics for each section are shown. Statistics for the sections are not clear due to bipolar distribution seen in the measurements.

Locality 1: Alkali Anticline: Total Height 497.25m			Statistics	
Height in Section	**Measurement**	**Description of Measurement**	n	75
63.3	0.4 / 315	Trough Cross Bedding	**Kuiper's test**	
63.3	0.3 / 123	Trough Cross Bedding	V_n	0.319
63.3	0.1 / 127	Trough Cross Bedding	$V_{0.05}$	0.198
63.3	0.2 / 344	Trough Cross Bedding	$V_{0.01}$	0.226
63.3	0.4 / 345	Trough Cross Bedding	$H_{0\ 0.05}$	rejected
63.3	0.1 /187	Trough Cross Bedding	$H_{0\ 0.01}$	rejected
63.3	0.3 / 239	Trough Cross Bedding	**Watson's test**	
63.3	0.4 / 231	Trough Cross Bedding	u^{*2}	0.386
63.3	0.3 / 358	Trough Cross Bedding	u^2	0.389
63.3	0.15 / 131	Trough Cross Bedding	$u^2_{0.05}$	0.187
63.3	0.2 / 278	Trough Cross Bedding	$u^2_{0.01}$	0.267
63.3	0.4 / 013	Trough Cross Bedding	$H_{0\ 0.05}$	rejected
63.3	0.4 / 317	Trough Cross Bedding	$H_{0\ 0.01}$	rejected
63.3	0.3 / 225	Trough Cross Bedding	**Rayleigh's test**	
63.3	0.1 / 311	Trough Cross Bedding	$\Sigma (\sin \theta_i)$	8.136
63.3	348	Wave Ripple Crest Trend	$\Sigma (\cos \theta_i)$	-8.243
63.3	348	Wave Ripple Crest Trend	$\Sigma (\tan \theta_i)$	-0.987
63.3	322	Wave Ripple Crest Trend	θ	-44.625
63.3	11	Wave Ripple Crest Trend	M	135.376
63.3	8	Wave Ripple Crest Trend	R	0.154
63.3	21	Wave Ripple Crest Trend	s_B	74.510
179.1	334	Wave Ripple Crest Trend	K	0.313
179.1	332	Wave Ripple Crest Trend	$R_{0.05}$	0.200
192.9	127	Ripple Cross Lamination	$R_{0.01}$	0.248
192.9	131	Ripple Cross Lamination	$H_{0\ 0.05}$	accepted
192.9	132	Ripple Cross Lamination	$H_{0\ 0.01}$	accepted
192.9	136	Ripple Cross Lamination	**Confidence sector of mean**	
255.8	355	Wave Ripple Crest Trend	$d°_{0.05}$	$n \cdot R \cdot K < 6$!
255.8	343	Wave Ripple Crest Trend	$d°_{0.01}$	$n \cdot R \cdot K < 6$!
255.8	320	Wave Ripple Crest Trend	**Distribution type**	
255.8	166	Ripple Cross Lamination	α=0.05	Uniform
255.8	183	Ripple Cross Lamination	α=0.01	Uniform
255.8	165	Ripple Cross Lamination		
255.8	145	Ripple Cross Lamination		
255.8	226	Ripple Cross Lamination		

Locality 1: Alkali Anticline Continued		
255.8	131	Ripple Cross Lamination
291.3	340	Wave Ripple Crest Trend
291.3	338	Wave Ripple Crest Trend
307.35	83	Wave Ripple Crest Trend
316.75	281	Wave Ripple Crest Trend
347.55	0.3/ 148	Trough Cross Bedding
347.55	0.3 / 151	Trough Cross Bedding
347.55	0.4 / 162	Trough Cross Bedding
388.05	285	Wave Ripple Crest Trend
416.35	0.2 / 126	Trough Cross Bedding
416.35	0.2 / 128	Trough Cross Bedding
416.35	0.6 / 222	Trough Cross Bedding
421.35	277	Wave Ripple Crest Trend
421.35	265	Wave Ripple Crest Trend
434.55	0.2 / 010	Trough Cross Bedding
434.55	0.3 / 070	Trough Cross Bedding
434.55	0.2 / 152	Trough Cross Bedding
434.55	0.3 / 167	Trough Cross Bedding
434.55	138	Ripple Cross Lamination
434.55	140	Ripple Cross Lamination
434.55	134	Ripple Cross Lamination
434.55	166	Ripple Cross Lamination
434.55	161	Ripple Cross Lamination
434.55	166	Ripple Cross Lamination
446.55	124	Ripple Cross Lamination
446.55	115	Ripple Cross Lamination
446.55	127	Ripple Cross Lamination
446.55	126	Ripple Cross Lamination
446.55	131	Ripple Cross Lamination
474.05	0.3 / 115	Trough Cross Bedding
474.05	0.3 / 308	Trough Cross Bedding
488.45	0.2 / 280	Trough Cross Bedding
488.45	0.3 / 293	Trough Cross Bedding
488.45	0.7 / 137	Trough Cross Bedding
489.55	0.5 / 117	Trough Cross Bedding
489.55	0.3 / 116	Trough Cross Bedding
489.55	0.2 / 121	Trough Cross Bedding
489.55	0.5 / 109	Trough Cross Bedding
489.55	0.3 / 111	Trough Cross Bedding
489.55	0.1 / 302	Trough Cross Bedding

Locality 2: Large Field: Total Height 516.1m		
Height in Section	**Measurement**	**Description of Measurement**
436 - 443	0.1/293	Trough Cross Bedding
437 - 443	0.3/134	Trough Cross Bedding
438 - 443	0.1/281	Trough Cross Bedding
439 - 443	0.1/091	Trough Cross Bedding
440 - 443	0.3/133	Trough Cross Bedding
441 - 443	.4/248	Trough Cross Bedding
442 - 443	0.3/112	Trough Cross Bedding
443 - 443	0.3/120	Trough Cross Bedding
444 - 443	0.3/117	Trough Cross Bedding
445 - 443	0.15/265	Trough Cross Bedding
446 - 443	0.2/121	Trough Cross Bedding
447 - 443	0.5/273	Trough Cross Bedding
448 - 443	0.7/262	Trough Cross Bedding

Statistics	
n	13
Kuiper's test	
V_n	0.439
$V_{0.05}$	0.457
$V_{0.01}$	0.523
$H_{0\ 0.05}$	accepted
$H_{0\ 0.01}$	accepted
Watson's test	
u^{*2}	0.178
u^2	0.181
$u^2_{0.05}$	0.187
$u^2_{0.01}$	0.267
$H_{0\ 0.05}$	accepted
$H_{0\ 0.01}$	accepted
Rayleigh's test	
$\Sigma (\sin \theta_i)$	0.178
$\Sigma (\cos \theta_i)$	-3.205
$\Sigma (\tan \theta_i)$	-0.055
θ	-3.148
M	176.830
R	0.247
s_B	70.318
K	0.510
$R_{0.05}$	n < 15 !
$R_{0.01}$	n < 15 !
$H_{0\ 0.05}$	accepted
$H_{0\ 0.01}$	accepted
Confidence sector of mean	
$d°_{\ 0.05}$	n·R·K < 6 !
$d°_{\ 0.01}$	n·R·K < 6 !
Distribution type	
α=0.05	Uniform
α=0.01	Uniform

Locality 3: Greybull Bench: Total Height 374.65m			Statistics	
Height in Section	**Measurement**	**Description of Measurement**	n	43
69.8	162	Ripple Cross Lamination	**Kuiper's test**	
69.8	150	Ripple Cross Lamination	V_n	0.440
69.8	144	Ripple Cross Lamination	$V_{0.05}$	0.259
86	150	Ripple Cross Lamination	$V_{0.01}$	0.296
86	145	Ripple Cross Lamination	$H_{0\ 0.05}$	rejected
86	146	Ripple Cross Lamination	$H_{0\ 0.01}$	rejected
86	150	Ripple Cross Lamination	**Watson's test**	
112.8	163	Ripple Cross Lamination	u^{*2}	0.860
112.8	172	Ripple Cross Lamination	u^2	0.874
112.8	130	Ripple Cross Lamination	$u^2_{0.05}$	0.187
112.8	0.3/192	Trough Cross Bedding	$u^2_{0.01}$	0.267
112.8	0.5/203	Trough Cross Bedding	$H_{0\ 0.05}$	rejected
112.8	0.2/204	Trough Cross Bedding	$H_{0\ 0.01}$	rejected
160.6	150	Ripple Cross Lamination	**Rayleigh's test**	
160.6	210	Ripple Cross Lamination	$\Sigma (\sin \theta_i)$	14.389
160.6	184	Ripple Cross Lamination	$\Sigma (\cos \theta_i)$	-21.352
160.6	212	Ripple Cross Lamination	$\Sigma (\tan \theta_i)$	-0.673
160.6	167	Ripple Cross Lamination	θ	-33.940
160.6	172	Ripple Cross Lamination	M	146.025
241.1	1.5/172	Trough Cross Bedding	R	0.599
272.3	0.15/238	Trough Cross Bedding	s_B	51.325
272.3	0.3/045	Trough Cross Bedding	K	1.476
302.1	0.3/240	Trough Cross Bedding	$R_{0.05}$	0.264
325.3	0.2/156	Trough Cross Bedding	$R_{0.01}$	0.327
325.3	0.2/118	Trough Cross Bedding	$H_{0\ 0.05}$	rejected
325.3	325	Wave ripple crest trend	$H_{0\ 0.01}$	rejected
352.7	0.3/121	Trough Cross Bedding	**Confidence sector of mean**	
360	0.5/103	Trough Cross Bedding	$d°_{0.05}$	18.166
360	1.2/094	Trough Cross Bedding	$d°_{0.01}$	24.005
360	0.8/350	Trough Cross Bedding	**Distribution type**	
360	0.33/064	Trough Cross Bedding	α=0.05	Von Mises
360	0.2/305	Trough Cross Bedding	α=0.01	Von Mises
360	0.3/065	Trough Cross Bedding		
360	0.8/112	Trough Cross Bedding		
368.7	0.4/100	Trough Cross Bedding		
368.7	0.3/080	Trough Cross Bedding		
368.7	0.3/049	Trough Cross Bedding		
368.7	1.0/128	Trough Cross Bedding		

Locality 3: Grey Bench Continued		
368.7	0.4/145	Trough Cross Bedding
368.7	0.4/159	Trough Cross Bedding
368.7	0.3/140	Trough Cross Bedding
368.7	0.7/151	Trough Cross Bedding
368.7	0.3/114	Trough Cross Bedding

Locality 4: Little Dry Creek: Total Height Accessible 137.17m			Statistics	
Height in Section	**Measurement**	**Description of Measurement**	n	7
30.2	0.6/140	Trough Cross Bedding	**Kuiper's test**	
30.2	0.2/129	Trough Cross Bedding	V_n	0.548
30.2	0.3/292	Trough Cross Bedding	$V_{0.05}$	0.605
74.47	0.2/116	Trough Cross Bedding	$V_{0.01}$	0.692
129.67	0.3/176	Trough Cross Bedding	$H_{0\ 0.05}$	accepted
137.17	40/174	Trough Cross Bedding	$H_{0\ 0.01}$	accepted
137.17	70/246	Trough Cross Bedding	**Watson's test**	
			u^{*2}	0.145
			u^2	0.148
			$u^2_{0.05}$	0.187
			$u^2_{0.01}$	0.267
			$H_{0\ 0.05}$	accepted
			$H_{0\ 0.01}$	accepted
			Rayleigh's test	
			$\Sigma (\sin \theta_i)$	0.652
			$\Sigma (\cos \theta_i)$	-3.858
			$\Sigma (\tan \theta_i)$	-0.168
			θ	-9.836
			M	170.403
			R	0.559
			s_B	53.812
			K	1.338
			$R_{0.05}$	n < 15 !
			$R_{0.01}$	n < 15 !
			$H_{0\ 0.05}$	accepted
			$H_{0\ 0.01}$	accepted
			Confidence sector of mean	
			$d°_{\ 0.05}$	n·R·K < 6 !
			$d°_{\ 0.01}$	n·R·K < 6 !
			Distribution type	
			α=0.05	Uniform
			α=0.01	Uniform

Locality 5: Casey's: Total Height 459.1m			Statistics	
Height in Section	**Measurement**	**Description of Measurement**	n	70
122.3	282	Along Ripple Crest	**Kuiper's test**	
122.3	144	Ripple Cross Lamination	V_n	0.515
122.3	141	Ripple Cross Lamination	$V_{0.05}$	0.205
122.3	156	Ripple Cross Lamination	$V_{0.01}$	0.234
122.3	170	Ripple Cross Lamination	$H_{0\ 0.05}$	rejected
122.3	136	Ripple Cross Lamination	$H_{0\ 0.01}$	rejected
122.3	182	Ripple Cross Lamination	**Watson's test**	
122.3	99	Ripple Cross Lamination	u^{*2}	1.507
122.3	93	Ripple Cross Lamination	u^2	1.523
122.3	0.15/215	Trough Cross Bedding	$u^2_{0.05}$	0.187
153	144	Ripple Cross Lamination	$u^2_{0.01}$	0.267
153	161	Ripple Cross Lamination	$H_{0\ 0.05}$	rejected
153	167	Ripple Cross Lamination	$H_{0\ 0.01}$	rejected
153	155	Ripple Cross Lamination	**Rayleigh's test**	
153	165	Ripple Cross Lamination	$\Sigma (\sin \theta_i)$	12.562
153	168	Ripple Cross Lamination	$\Sigma (\cos \theta_i)$	-35.746
186	135	Ripple Cross Lamination	$\Sigma (\tan \theta_i)$	-0.351
186	162	Ripple Cross Lamination	θ	-19.341
186	182	Ripple Cross Lamination	M	160.638
186	165	Ripple Cross Lamination	R	0.541
186	159	Ripple Cross Lamination	s_B	54.880
186	1.4/142	Trough Cross Bedding	K	1.280
224	135	Ripple Cross Lamination	$R_{0.05}$	0.207
224	162	Ripple Cross Lamination	$R_{0.01}$	0.257
224	162	Ripple Cross Lamination	$H_{0\ 0.05}$	rejected
224	165	Ripple Cross Lamination	$H_{0\ 0.01}$	rejected
224	159	Ripple Cross Lamination	**Confidence sector of mean**	
253	0.2/156	Trough Cross Bedding	$d°_{0.05}$	16.084
253	126	Ripple Cross Lamination	$d°_{0.01}$	21.254
253	130	Ripple Cross Lamination	**Distribution type**	
253	143	Ripple Cross Lamination	α=0.05	Von Mises
253	152	Ripple Cross Lamination	α=0.01	Von Mises
253	146	Ripple Cross Lamination		
284.4	0.2/171	Trough Cross Bedding		
284.4	0.2/170	Trough Cross Bedding		
284.4	0.2/157	Trough Cross Bedding		
326.7	200	Ripple Cross Lamination		

Locality 5: Casey's Continued		
326.7	188	Ripple Cross Lamination
326.7	198	Ripple Cross Lamination
326.7	202	Ripple Cross Lamination
326.7	295	Wave Ripple Trend
349	0.4/175	Trough Cross Bedding
349	0.3/152	Trough Cross Bedding
349	0.3/148	Trough Cross Bedding
349	0.8/152	Trough Cross Bedding
349	0.4/161	Trough Cross Bedding
349	0.3/173	Trough Cross Bedding
349	0.4/158	Trough Cross Bedding
349	0.5/159	Trough Cross Bedding
349	0.3/140	Trough Cross Bedding
378	0.15/007	Trough Cross Bedding
378	0.15/346	Trough Cross Bedding
378	0.15/025	Trough Cross Bedding
395.3	0.2/172	Trough Cross Bedding
395.3	0.1/359	Trough Cross Bedding
395.3	0.15/182	Trough Cross Bedding
395.3	0.2/351	Trough Cross Bedding
447.6	0.2/144	Trough Cross Bedding
447.6	0.3/141	Trough Cross Bedding
447.6	0.6/177	Trough Cross Bedding
447.6	0.4/322	Trough Cross Bedding
447.6	0.2/328	Trough Cross Bedding
447.6	0.2/325	Trough Cross Bedding
447.6	0.2/247	Trough Cross Bedding
447.6	1.0/326	Trough Cross Bedding
459.1	0.3/300	Trough Cross Bedding
459.1	0.4/319	Trough Cross Bedding
459.1	0.3/203	Trough Cross Bedding
459.1	0.3/036	Trough Cross Bedding
459.1	0.3/060	Trough Cross Bedding